

# **Acoustic Black Holes and Superresonance Mechanisms**

**Sofia Ferro Freitas**

Thesis to obtain the Master of Science Degree in

**Engineering Physics**

Supervisor: Prof. Dr. Vítor Manuel dos Santos Cardoso

## **Examination Committee**

Chairperson: Prof. Dr. Ana Maria Vergueiro Monteiro Cidade Mourão

Supervisor: Prof. Dr. Vítor Manuel dos Santos Cardoso

Member of the Committee: Dr. David Mathew Hilditch

**October 2017**



Para os meus pais.



## Acknowledgements

An attempt at saying thank you is better than no attempt at all. So here is my two cents, following the "Friends, Family and Fools" motto.

To my family, I owe you a huge thanks. To my parents, to whom I dedicate this thesis, all of this is possible thanks to you. For their will of character, perseverance and moral grounds, I am tremendously grateful. To all my cousins, uncles and aunts, grandparents and family friends, I appreciate all the support and availability.

Friends... Ah, imagine a life with no friends? Boring, dull, gloomy, purposeless. I am glad mine is none of those attributes. Thank you for bringing diversity and adventure to my life. And on that note, a special thank you to *Turno da Noite* – careful, now that we are being mentioned in official papers we are on the verge of becoming a cult! –, for all the memorable moments.

And finally the fool, my supervisor Vítor Cardoso, who accepted to work with me – and who I sincerely hope that finds this funny rather than offensive. Doing this thesis has been a truly enriching experience, and my supervisor has undoubtedly played a major role in that. For all the good advice, geniality, perfectionism and knowledge, for the ability of levelling down and being an outstanding teacher, a monumental thank you.



## Resumo

Todos nós estamos familiarizados, de certa forma, com a definição de um horizonte de eventos. Inúmeros trabalhos de ficção científica estiveram na base da difusão desta noção de pontos de não-retorno na cultura popular. O que é talvez desconhecido à maioria do público é a facilidade com que se pode reproduzir características de buracos negros. Mais concretamente, o quão fácil é encontrar outros sistemas físicos com horizontes. De facto, foi demonstrado que ondas de som, num fluido em movimento, se comportam de forma análoga a campos escalares em espaços-tempo curvos. Fluidos supersónicos podem gerar "buracos mudos", que correspondem a regiões do espaço a partir das quais não é possível extrair qualquer informação. Este é o análogo de um buraco negro na teoria de Relatividade Geral.

Esta equivalência matemática é muito poderosa uma vez que permite estudar buracos negros em laboratórios. Em particular, é possível analisar o problema de superradiância – um processo de magnificação de radiação que resulta na amplificação de ondas incidentes em buracos negros em rotação.

Nesta tese, revemos o trabalho feito em análogos acústicos num potencial de ralo de banheira. Usamos este modelo para estudar as condições para superradiância bem como a estabilidade das suas soluções. Também analisamos uma segunda montagem, que consiste num cilindro em rotação como possível fonte de amplificação. Finalmente, incorporamos viscosidade no fluido de fundo e estudamos de que forma os resultados são afetados.

**Palavras-chave:** Superradiância, Análogos Acústicos, Mecânica de Fluidos, Relatividade Geral, Geometrias Acústicas Confinadas, Viscosidade.



## Abstract

We are all somehow familiar with the definition of an event horizon. Science fiction works have greatly contributed to the widespread knowledge of these points of no return in spacetime amongst the general public. What is perhaps unknown to most is how easily one can reproduce characteristics of black holes. More precisely, how easy it is to find other physical systems also displaying horizons. Indeed, it has been showed that sound waves, in a moving fluid, behave analogously to scalar fields in a curved spacetime. Supersonic fluid flow can generate a "dumb hole", which corresponds to a region in space from which no information can be extracted. This is the analogue of a black hole in the theory of General Relativity.

The formal mathematical equivalence is very powerful once it allows for the study of black holes in laboratories. In particular, it is possible to contemplate the problem of superradiance – a radiation enhancement process that results in the amplification of incoming waves in rotating black holes.

In this thesis, we review the work done in acoustic analogues for a draining bathtub flow. We use this toy model to study the conditions for superradiance and the stability of the solutions. We also look at a different setup, consisting of a rotating cylinder as a possible source of amplification. Lastly, we incorporate viscosity in the background fluid and study how the results are affected.

**Keywords:** Superradiance, Acoustic Analogues, Fluid Mechanics, General Relativity, Confined Acoustic Geometries, Viscosity.



# Contents

Acknowledgments . . . . .	v
Resumo . . . . .	vii
Abstract . . . . .	ix
List of Tables . . . . .	xiii
List of Figures . . . . .	xv
Nomenclature . . . . .	xvii
<b>1 Introduction</b>	<b>1</b>
1.1 Motivation and overview . . . . .	1
1.2 Objectives . . . . .	5
1.3 Thesis outline . . . . .	5
<b>2 Acoustic Analogues</b>	<b>7</b>
2.1 Fluid dynamics . . . . .	7
2.2 Vortex geometries: the draining bathtub fluid flow . . . . .	10
<b>3 Dynamics of Acoustic Holes</b>	<b>13</b>
3.1 Wave equation . . . . .	13
3.2 Wave dispersion relation . . . . .	14
3.3 Scattering in the vortex geometry. Superradiance . . . . .	15
3.4 Quasinormal modes and stability . . . . .	18
<b>4 Dynamics of Acoustic Geometries</b>	<b>21</b>
4.1 Wave equation . . . . .	21
4.2 Scattering off a rotating cylinder. Superradiance . . . . .	22
4.3 Quasinormal modes and stability . . . . .	25
4.4 Confined geometry . . . . .	28
<b>5 Dynamics of Acoustic Geometries in Viscous Flows</b>	<b>31</b>
5.1 Governing equations and wave equation . . . . .	31
5.2 Wave dispersion relation . . . . .	34
5.3 Scattering in the presence of viscosity . . . . .	34
5.4 Quasinormal modes. Superradiant instabilities in the presence of viscosity . . . . .	37

5.5	Confined geometry in the presence of viscosity . . . . .	38
<b>6</b>	<b>Conclusions</b>	<b>41</b>
6.1	Achievements . . . . .	41
6.2	Future work . . . . .	43
	<b>Bibliography</b>	<b>45</b>
<b>A</b>	<b>The potential barrier</b>	<b>51</b>

# List of Tables

3.1	Fundamental quasinormal frequencies, for $B = 0$ .	20
4.1	$\Omega$ that maximises the reflection coefficient $ R_{\omega m} ^2$ .	24
4.2	Frequencies of QNMs.	27
4.3	Fit parameters for the plots displayed in Figure 4.9.	28
5.1	Viscosity $\hat{\alpha}$ of known materials at room temperature.	34
A.1	Points of interest from Figure A.1.	53



# List of Figures

1.1	Schematic description of the Penrose process in a Kerr BH. . . . .	3
1.2	Propagation of information using the analogue fluid mechanics. . . . .	4
2.1	Scheme of the different regions of a BH in the fluid analogy. . . . .	10
2.2	Vortex used to study the draining bathtub spacetime. . . . .	11
3.1	Reflection coefficient $ R_{\omega m} ^2$ as a function of $\omega$ . . . . .	18
3.2	Gist of the numerical method of direct integration used to compute the QNMs. . . . .	19
4.1	Reflection coefficient $ R_{\omega m} ^2$ as a function of $\omega$ . . . . .	23
4.2	Reflection coefficient $ R_{\omega m} ^2$ as a function of $\omega$ for $\Omega \leq 1$ . . . . .	24
4.3	Reflection coefficient $ R_{\omega m} ^2$ as a function of $\omega$ for $Z = 0.1(1 - i)$ . . . . .	24
4.4	Reflection coefficient $ R_{\omega m} ^2$ as a function of $\omega$ for $Z = 10(1 - i)$ . . . . .	25
4.5	Reflection coefficient $ R_{\omega m} ^2$ as a function of $\omega$ for $\Omega = 0.7 c/R_0$ and different acoustic impedances. . . . .	25
4.6	Pictorial view of the confined setup. . . . .	26
4.7	Real and imaginary parts of the frequency $\omega$ as functions of the confinement radius $R_1/R_0$ . . . . .	26
4.8	Reflection coefficient $ R_{\omega m} ^2$ as a function of $\omega$ , where we show the correspondence with the QNMs. . . . .	27
4.9	Linear regressions for the values of frequency of the QNMs, real and imaginary. . . . .	28
4.10	Imaginary part of the frequency versus the radius $R_1/R_0$ . . . . .	29
4.11	Coordinates $R_1/R_0$ and $\Omega$ for which $\omega_I = 0$ . . . . .	29
5.1	Reflection coefficient $ R_{\omega m} ^2$ as a function of $\omega$ . . . . .	36
5.2	Area normalisation. . . . .	37
5.3	Real and imaginary parts of the frequency for the QNMs. . . . .	37
5.4	Offset of the real and imaginary parts of the frequency for the QNMs with respect to the non-viscous case. . . . .	38
5.5	Imaginary part of the frequency as a function of the ratio $R_1/R_0$ , for several values of viscosity. . . . .	39
A.1	Potential and test energies for the different values of $m$ . . . . .	52
A.2	Scattering experiment with two different incoming waves, carrying $E_1$ and $E_2$ . . . . .	52



# Nomenclature

## Abbreviations and acronyms

BH Black Hole.

GR General Relativity.

QNM Quasinormal mode.

## Greek symbols

$\alpha$  Viscosity coefficient. It is defined as a linear combination of the dynamic and bulk viscosity coefficients,  $\alpha = \xi + \frac{4}{3}\mu$ .

$\Omega$  Angular velocity, referring either to the angular velocity at the black hole horizon or at the radius of the cylinder.

$\omega$  Wave frequency.

$\psi$  Velocity potential, defined via  $\mathbf{v} = \nabla\psi$ .

$\rho$  Density of the background fluid.

$\theta$  Angular variable in polar coordinates.

## Roman symbols

$\mathbf{v}$  Fluid velocity vector field.

$c$  Speed of sound in the fluid.

$H$  Enthalpy.

$h$  Specific enthalpy, defined as the enthalpy per unit mass.

$m$  Azimuthal number. It is the projection of the angular momentum in the direction of propagation of the wave.

$p$  Pressure of the fluid.

$r$  Radial variable in polar coordinates.

$S$  Entropy.

$T$  Temperature.

$V$  Volume.

$Z$  Acoustic impedance. It dictates the interactions wall-wave in the cylinder spacetime. A detailed explanation is provided in Section 4.2.

### **Superscripts**

$\dagger$  Transpose conjugate.

$T$  Transpose.

# Chapter 1

## Introduction

### 1.1 Motivation and overview

John A. Wheeler first coined the term “black hole” in 1967 to describe an object resulting from gravitational collapse [1]: “A black hole is what is left behind after an object has undergone complete gravitational collapse. Spacetime is so strongly curved that no light can come out, no matter can be ejected, and no measuring rod can ever survive without being put in. Any kind of object that falls into the black hole loses its separate identity, preserving only its mass, charge, angular momentum, and linear momentum.”

Black holes (BHs) are described by the theory of General Relativity (GR). GR was developed in 1915 by Albert Einstein and it describes gravity as the curvature of spacetime. In 1904, Einstein was troubled by the views of relativity put forward by Galileo and Maxwell. On the one hand, Galileo claimed that absolute motion could not be defined. Maxwell’s electromagnetism, on the other hand, established that light travelled at a fixed speed  $c$ . Einstein came to the conclusion these two notions could only be compatible if  $c$  were to be kept constant in different frames of reference. The subsequent view that time was not absolute made way for the establishment of Special Relativity. GR arose years later, expanding the theory to account for effects of acceleration. The latter passed its first test in 1919, when the bending of star light was observed during a solar eclipse [2]. Since then, the theory has been put to test in several other occasions, the latest being the experimental detection of gravitational waves in 2015 [3]. In a nutshell, GR is defined via Einstein’s field equations,

$$G_{\mu\nu} = R_{\mu\nu} - \frac{1}{2}Rg_{\mu\nu} = 8\pi T_{\mu\nu}, \quad (1.1)$$

which describe how matter and energy interact with spacetime, the fabric of our universe. The Ricci tensor  $R_{\mu\nu}$  and the Ricci scalar  $R = g^{\mu\nu}R_{\mu\nu}$  are geometrical entities which measure the curvature of spacetime. They depend solely on the metric  $g_{\mu\nu}$ . The element on the RHS of the equation,  $T_{\mu\nu}$ , is the stress-energy tensor and it accounts for the presence and distribution of matter.

The challenge with Einstein’s equations is finding a metric that satisfies them, given physically rea-

sonable matter. The first person to come up with such a metric was Karl Schwarzschild. In January 1916, he computed the gravitational field generated by a static point mass and realised it satisfied Einstein's equations. Schwarzschild's metric yielded the simplest known BH, one with no electric charge or angular momentum [4]. According to Birkhoff's theorem, the Schwarzschild metric is the most general spherically symmetric vacuum solution of the Einstein's field equations. Subsequently, other solutions have been discovered. A particularly relevant one for this work is the Kerr solution, which describes a rotating BH. The Kerr metric was discovered in 1963 by Roy Kerr and it reads

$$ds^2 = - \left( 1 - \frac{2GM}{r} \right) dt^2 - \frac{4GMa \sin^2 \theta}{\rho^2} dt d\phi + \frac{\rho^2}{\Delta} dr^2 + \rho^2 d\theta^2 + \frac{\sin^2 \theta}{\rho^2} [(r^2 + a^2)^2 - a^2 \Delta \sin^2 \theta] d\phi^2, \quad (1.2)$$

where  $\Delta$  and  $\rho^2$  are defined as

$$\Delta = r^2 - 2GM r + a^2 \quad (1.3)$$

$$\rho^2 = r^2 + a^2 \cos^2 \theta. \quad (1.4)$$

$M$  is the mass of the BH and  $a$  is the angular momentum per unit mass. These two quantities parametrise the possible solutions, or equivalently, the possible Kerr BHs. The Kerr metric inspired the formulation of the uniqueness theorems, developed by Israel, Price, Carter, Robinson and Hawking, amongst others [5]. The uniqueness theorems refer to the existence of solutions to the Einstein field equations under certain conditions. The first BH uniqueness theorem is due to Israel who, in 1967, proved that a static, topologically spherical BH is described by the Schwarzschild [6] or the Reissner-Nördström [7] solutions. A very important theorem in BH physics is the no-hair theorem. It postulates that given the mass, electric charge and angular momentum of a BH, its properties are fully determined. This theorem is behind Wheeler's famous phrase that "black holes have no hair".

Despite its extremely interesting features, astrophysical BHs are of difficult observation and direct study. That is why one must rely on other, secondary, effects. A very important secondary effect is the Penrose process. Theorised in 1969 by Roger Penrose, it accounts for the loss of angular momentum in rotating BHs. Penrose argued that once particles entered a special region of the BH, called the ergosphere, they could be scattered and ejected with greater energy than the one they had initially. Such process is illustrated in Figure 1.1. A precise definition of the ergosphere is left to Chapter 2. Note that this scattering process rarely occurs, as very specific conditions must be verified. Nonetheless, the Penrose process was central in the establishment of its analogue wave process, superradiance. Superradiance is a radiation enhancement process that occurs in dissipative systems. In the particular case of BHs, it happens at the level of the event horizon. Superradiance allows for energy and angular momentum to be extracted from the vacuum, resulting in a consequent amplification of the scattered wave packet. Superradiance in rotating BHs was first discovered in 1971, by Zel'dovich. He showed, provided the superradiance condition is satisfied, that the scattering of incident waves in rotating dissipative bodies resulted in an amplification of such waves, producing outgoing waves of larger amplitude.

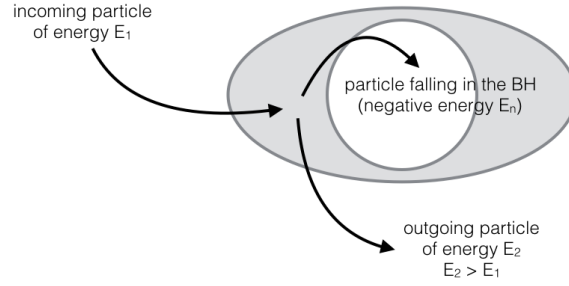


Figure 1.1: Schematic description of the Penrose process in a Kerr BH, in which the outgoing particle has energy  $E_2 > E_1$ . The ergosphere corresponds to the region in grey, limited by the ergosurface and the BH horizon (respectively the outer and inner limits).

The superradiance condition reads

$$\omega < m\Omega, \quad (1.5)$$

where  $\omega$  is the frequency of the incident radiation,  $m$ , the azimuthal number, accounts for the projection of the angular momentum along the axis of rotation and  $\Omega$  is the angular velocity of the body. It has been showed that only bosonic perturbations yield superradiance. The reason behind why fermionic fields cannot produce superradiance has to do with Pauli's exclusion principle. In fact, one can interpret superradiance as a spontaneous pair production phenomenon [8]. Pauli's exclusion principle limits the number of fermionic pairs with the same quantum numbers, whereas the number of bosonic pairs has no such limitation. When computing the ratio between the amplitudes of the reflected and incident waves, one arrives at the conclusion that such ratio is never greater than the unity in the fermionic case. This limitation is present even under the condition of equation (1.5). Thus, superradiance is present for scalar, electromagnetic and gravitational perturbations, but absent for fermionic perturbations. A very fascinating application of BH superradiance worth mentioning is the BH bomb. Suppose we add a perfectly reflecting wall outside a Kerr BH. Consecutive amplification of the waves at the horizon gives rise to superradiant instabilities. Such instabilities may be observed, for instance, in massive bosonic fields, where the mass term acts as an effective potential barrier for superradiant modes. In 1974, Stephen Hawking, looking at quantum corrections to the scattering of waves in the event horizon, discovered that BHs radiate. An interesting consequence of Hawking's result is that BHs are not completely black. Instead, they emit thermal radiation, analogously to the one emitted by a black body of temperature proportional to the area of the Kerr BH. Thermal emission from BHs has been extensively studied by many physicists in a variety of ways, including DeWitt, Unruh, Wald, Parker and Bekenstein. Bekenstein was the first to defend the existence of BH thermal emission, based solely on thermodynamics arguments [9]. Another feature of the Penrose process is that it ultimately results in BH evaporation. In other words, BHs radiate out all of their energy until they eventually vanish. For an extensive read on superradiance see Reference [10].

In 1981, Unruh showed that sound waves, in a moving fluid, behave the same way as scalar fields in curved spacetimes [11]. He observed horizons could occur in day-to-day situations and drew analogies between fluid mechanics and GR. He called these horizons "dumb holes", and proved their existence

was a consequence of supersonic fluid flows, as illustrated in Figure 1.2. By finding ways to reproduce

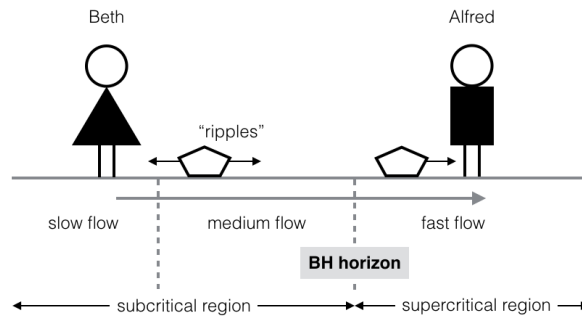


Figure 1.2: Propagation of information using the analogue fluid mechanics. Beth and Alfred communicate using "ripples" (acoustic disturbances) in the free surface of the fluid. The fluid naturally flows from Beth to Alfred, so she is always able to get her message across. For Alfred to be able to reply to Beth, he must be able to guarantee the ripples he sends move faster upstream than the flow does downstream. But Alfred is in a supercritical region, so he can never send any information upstream – nothing can counterpropagate the flow in this region. Hence, the region separating the sub and supercritical regions is the analogue BH horizon.

behaviours of BHs and other astrophysical bodies, one is able to carry out experiments in laboratories, with the aim of testing the existing theories.

Throughout this thesis, we will be working in the context of analogue gravity as a means of making predictions for experiments. A leading laboratory in the field is the Quantum Gravity Laboratory in Nottingham, which has set as its goal to put together experiments that can help gather insights on gravity and analogues. It simultaneously serves as a testing vessel for quantum field theory in curved spacetimes and as motivation for the development of new areas of physics – such as analogue gravity. In a recent article [12], Silke Weinfurtner's team describes the first laboratory detection of superradiance. By working with a draining bathtub fluid flow, they observed that plane waves propagating on the surface of the water were amplified after being scattered off by the draining vortex. The experimental setup in Nottingham was first described in 2002 by Unruh and Schützhold [13]. They proposed an experiment in which superradiance could be detected in the laboratory by assuming a long wavelength, shallow water approximation. An alternative experimental setup worth mentioning is the one proposed by Cardoso et al., in 2016 [14]. The authors analysed the hypothesis of mimicking the vortex geometry by making use of a rotating cylinder. They showed that, given an appropriate choice of material for the cylinder, surface and sound waves were amplified. We analyse both proposals in this thesis.

At last, we refer to three particular works displaying the broad scope of study of analogue gravity. We first draw our attention to an article by Pelloquin et al., where the scenario of a traversable and bidirectional wormhole is discussed [15]. In GR, wormholes are non-traversable, closing up too quickly. The description of an analogue wormhole, on the other hand, can encompass any velocity profile and hence allows for more general results. The second paper we analyse is by Steinhauer [16]. The author looks at how the experimental realisation of an analogue BH laser allows for the observation of Hawking radiation. An analogue BH laser consists of a cavity encompassed by a BH and a white hole. Picture an actual laser, composed by a light beam reflected back and forth inside an optical cavity – Figure 7 in

Reference [17] provides a good overview on the subject. Finally, we see how spintronics can be used to create analogue horizons [18]. The authors' goal is realising a BH with magnons, the quanta of spin waves. The spin-wave velocity is used as the critical speed above which no information can be retrieved, instead of the speed of sound .

## 1.2 Objectives

The aim of this thesis is to provide the reader with the current state-of-the-art of analogues for the detection of superradiance. We seek to examine how superradiance occurs in several setups whilst looking at the stability of the solutions. Furthermore, we examine whether horizons are a necessary condition for superradiance. A major goal of our work is including viscosity in an already well-established treatment of analogue gravity that assumes non-viscous fluids. We explore setups that have not yet been realised experimentally and hence another objective of the work is to make predictions that can later be compared against experiment.

## 1.3 Thesis outline

In this thesis, the first two chapters are dedicated to explaining the important concepts regarding both superradiance and analogue gravity. Chapter 1 provides an overview on superradiance, including a state-of-the-art analysis and the fundamental notions and motivation behind its study. In Chapter 2, the framework of analogue gravity is presented. Chapter 3 deals with the dynamics of acoustic holes. We present an analysis on the quasinormal modes (QNMs), as well as results for superradiance in a  $(1+2)$ -dimensional bathtub flow spacetime. In Chapter 4, we look at a different setup, in which superradiance can be studied in situations where no horizons arise, by means of a rotating cylinder. We study the scattering and later confine the setup by adding an external wall. One verifies superradiant instabilities arise in the latter. Chapter 5 renders an analysis on how viscosity impacts the QNMs frequencies and the superradiance results. Lastly, Chapter 6 features the final conclusions, as we examine the achievements of the work developed in the thesis. A list of future extensions is also provided. Throughout this work, whenever possible, we complete the theoretical predictions with the corresponding numerical results.



# Chapter 2

## Acoustic Analogues

In this chapter, we guide the reader through the topic of acoustic analogues. In essence, one will show that sound waves propagate within a fluid in the same way as scalar fields do in a curved spacetime. If the fluid velocity exceeds the local speed of sound, the effective curved spacetime has an horizon.

### 2.1 Fluid dynamics

In 1981, Unruh developed a method for mapping certain aspects of BH physics into fluid mechanics. He started by considering a barotropic and inviscid fluid, whose flow is irrotational – though possibly time dependent. The equation of motion for the velocity potential describing an acoustic disturbance is identical to the d'Alembertian equation of motion for a minimally-coupled massless scalar field propagating in a  $(1 + 3)$ -dimensional Lorentzian geometry,

$$\Delta\psi = \frac{1}{\sqrt{-g}} (\partial_\mu \sqrt{-g} g^{\mu\nu} \partial_\nu \psi) = 0, \quad (2.1)$$

which is just the Klein Gordon equation,  $\nabla_\mu \nabla^\mu \psi = 0$ , describing the dynamics of a scalar field. Under these conditions, the propagation of sound is governed by an acoustic metric  $g_{\mu\nu}(t, \mathbf{x})$ , which depends algebraically on the density and velocity of the flow and on the local speed of sound in the fluid:

$$g_{\mu\nu}(t, \mathbf{x}) = \frac{\rho}{c} \begin{pmatrix} -(c^2 - \|\mathbf{v}\|^2) & -\mathbf{v}^T \\ -\mathbf{v} & I_{[3 \times 3]} \end{pmatrix}, \quad (2.2)$$

where  $I_{[3 \times 3]}$  is the  $3 \times 3$  identity matrix. In general, when the fluid is non-homogeneous and flowing, the acoustic Riemann tensor associated with the acoustic metric is non-zero.

There are two fundamental equations ruling fluid dynamics, the continuity equation and the Euler equation, respectively:

$$\partial_t \rho + \nabla \cdot (\rho \mathbf{v}) = 0 \quad (2.3)$$

$$\rho \frac{d\mathbf{v}}{dt} = \rho [\partial_t \mathbf{v} + (\mathbf{v} \cdot \nabla) \mathbf{v}] = \mathbf{F}, \quad (2.4)$$

where  $\rho$  is the density of the fluid and  $\mathbf{v}$  is the fluid velocity vector field.  $\mathbf{F}$  in the Euler equation is defined as

$$\mathbf{F} = -\nabla p - \rho \nabla \Phi, \quad (2.5)$$

$p$  being the pressure and  $\Phi$  the potential of an external driving force. We assume the fluid to be vorticity free, i.e. the fluid is locally irrotational. This means the velocity can be written as  $\mathbf{v} = \nabla \psi$ . By definition, vorticity free means the rotational is null, i.e.  $\nabla \times \mathbf{v} = 0$ . It is a well-known fact that  $\nabla \times (\nabla \psi) = 0$ , where  $\psi$  is a scalar field. This justifies the definition used. Furthermore, the fluid is assumed to be barotropic, meaning the fluid's equation of state is of the form  $\rho = \rho(p)$ . Such assumption is helpful in defining the specific enthalpy. The definition of enthalpy reads

$$dH = TdS + Vdp \quad (2.6)$$

and, as the fluid elements undergo reversible thermodynamic changes ( $dS = 0$ ), one can write the specific enthalpy as

$$h(p) = \int_0^p \frac{dp'}{\rho(p')}. \quad (2.7)$$

Integration of the latter yields

$$\nabla h = \frac{1}{\rho} \nabla p. \quad (2.8)$$

The Euler equation (2.4) is then reduced to

$$\partial_t \psi + h + \frac{1}{2} (\nabla \psi)^2 + \Phi = 0. \quad (2.9)$$

A wave can be thought of as some fundamental average bulk motion summed up with other higher order motions, which work as correction terms to the fundamental one. A very simple example that can help us understand this makes use of a musical instrument. Think of the sound emitted by a guitar string. It is not pure. In fact, playing an A note ( $f = 440$  Hz) on a guitar will actually result in a sound composed of the following frequencies: 440 Hz, 880 Hz, 1320 Hz, etc.  $f = 440$  Hz is the fundamental frequency, much as the bulk motion aforementioned. The remaining frequencies are those of higher harmonics. What we will be doing next is in all similar to the Fourier analysis described above. We linearise the fundamental equations around an average bulk motion described by the background dynamical quantities  $(p_0, \rho_0, \psi_0)$ , plus some low amplitude acoustic perturbations  $(\varepsilon p_1, \varepsilon \rho_1, \varepsilon \psi_1)$ . The infinite series are truncated to first order corrections:

$$p = p_0 + \varepsilon p_1 + \mathcal{O}(\varepsilon^2), \quad \rho = \rho_0 + \varepsilon \rho_1 + \mathcal{O}(\varepsilon^2), \quad \psi = \psi_0 + \varepsilon \psi_1 + \mathcal{O}(\varepsilon^2). \quad (2.10)$$

Hence, the continuity and the Euler equation can be rewritten as two versions of themselves: an unperturbed and a perturbed one. The unperturbed equations will simply be equations (2.3) and (2.9),

previously presented. The perturbed equations read

$$\text{Continuity equation: } \quad \partial_t \rho_1 + \nabla \cdot (\rho_1 \mathbf{v}_0 + \rho_0 \mathbf{v}_1) = 0 \quad (2.11)$$

$$\text{Euler equation: } \quad \partial_t \psi_1 + h_1 + \mathbf{v}_0 \nabla \psi_1 = 0, \quad (2.12)$$

where the perturbation to the enthalpy can be identified as  $h_1 = \frac{p_1}{\rho_0}$  via a Taylor expansion,

$$h \equiv h(p) = h(p_0 + \varepsilon p_1) = h(p_0) + \varepsilon p_1 \left. \frac{\partial h}{\partial p} \right|_{p=p_0} = h(p_0) + \varepsilon \frac{p_1}{\rho_0} \equiv h_0 + \varepsilon h_1. \quad (2.13)$$

Notice also  $\mathbf{v}_0 = \nabla \psi_0$  and  $\mathbf{v}_1 = \nabla \psi_1$ . Using the perturbed Euler equation (2.12), one is able to write  $p_1$  as a function of  $\rho_0$ ,  $\mathbf{v}_0$  and  $\psi_1$ ,

$$p_1 = -\rho_0 (\partial_t \psi_1 + \mathbf{v}_0 \nabla \psi_1). \quad (2.14)$$

Together with the barotropic assumption,

$$p = p(\rho) \implies p_1 = \frac{\partial p}{\partial \rho} \rho_1, \quad (2.15)$$

and the perturbed continuity equation (2.11), the following wave equation arises:

$$\partial_t \left( \frac{\partial \rho}{\partial p} \rho_0 (\partial_t \psi_1 + \mathbf{v}_0 \cdot \nabla \psi_1) \right) + \nabla \cdot \left( -\rho_0 \nabla \psi_1 + \frac{\partial \rho}{\partial p} \rho_0 \mathbf{v}_0 (\partial_t \psi_1 + \mathbf{v}_0 \cdot \nabla \psi_1) \right) = 0. \quad (2.16)$$

This wave equation describes the propagation of the linearised scalar potential  $\psi_1$ . Once  $\psi_1$  is computed,  $p_1$  and  $\rho_1$  are easily calculated via equations (2.14) and (2.15). Thus, the wave equation completely determines the propagation of the acoustic disturbances  $(p_1, \rho_1, \psi_1)$ . The background fields  $(p_0, \rho_0, \psi_0)$ , which appear as time-dependent and position-dependent coefficients in the equation, are constrained to solve the equations of fluid motion for an externally-driven, barotropic, inviscid, and irrotational flow. Defining the local speed of sound in the fluid as

$$c^{-2} = \frac{\partial \rho}{\partial p}, \quad (2.17)$$

we arrive at the wave equation

$$\partial_t (\rho_0 (\partial_t \psi_1 + \mathbf{v}_0 \cdot \nabla \psi_1)) + \nabla \cdot (-c^2 \rho_0 \nabla \psi_1 + \rho_0 \mathbf{v}_0 (\partial_t \psi_1 + \mathbf{v}_0 \cdot \nabla \psi_1)) = 0, \quad (2.18)$$

whose corresponding acoustic metric reads:

$$g_{\mu\nu}(t, \mathbf{x}) = \frac{\rho}{c} \begin{pmatrix} -(c^2 - v^2) & -\mathbf{v}^T \\ -\mathbf{v} & I_{[3 \times 3]} \end{pmatrix}.$$

For a more complete discussion, see Reference [19]. Note the author uses a different convention for the sign of the velocity potential  $\mathbf{v} = -\nabla \psi$ , symmetric to the one used in this thesis.

Besides the acoustic metric, there is a physical spacetime metric, which is the usual flat Minkowski,

$$\eta_{\mu\nu} = \text{diag}(-c_{\text{light}}^2, 1, 1, 1). \quad (2.19)$$

The fluid particles couple only to the physical metric  $\eta_{\mu\nu}$ . Actually, the fluid motion is completely non-relativistic:  $\|\mathbf{v}_0\| \ll c_{\text{light}}$ . On the other hand, the acoustic perturbations couple only to the acoustic metric  $g_{\mu\nu}$ .

The goal of doing this analogue gravity treatment, as already hinted in Chapter 1, is using it in BH physics. Bearing that in mind, we present next the definition of the analogues for horizons and ergoregions. Assuming a steady flow – which corresponds to considering a stationary BH – the time translation Killing vector reads

$$K^\mu = \partial_t^\mu = (1, 0, 0, 0)^\mu. \quad (2.20)$$

An ergosurface is defined as the region of space where the norm of the timelike Killing vector is null, i.e.

$$K^\mu K_\mu = g_{\mu\nu} K^\mu K^\nu = g_{tt} = 0 \quad (2.21)$$

which, in the acoustic metric defined in equation (2.2), corresponds to the following condition:

$$\|\mathbf{v}\| = c. \quad (2.22)$$

Consequently, the ergosphere – region of space with the ergosurface as an outer boundary – occurs whenever the flow is supersonic,  $\|\mathbf{v}\| > c$ . The future event horizon, as in GR, is defined by demanding that it is the boundary from which null geodesics cannot escape. Particles moving along null geodesics – curves characterised by  $ds^2 = 0$  – are phonons and photons, respectively in the analogue and in GR. A past event horizon, on the other hand, is defined in terms of the region that cannot be reached from incoming particles moving along null geodesics. The regions of interest are summarised in Figure 2.1.

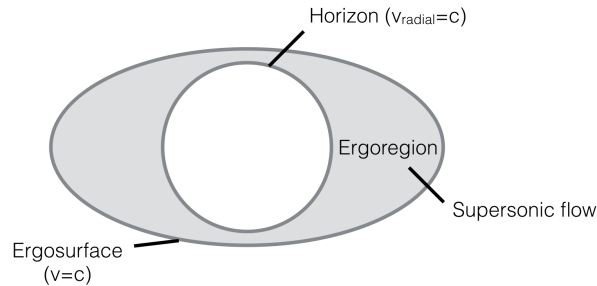


Figure 2.1: Scheme of the different regions of a BH in the fluid analogy.

## 2.2 Vortex geometries: the draining bathtub fluid flow

Using the fluid treatment previously introduced, we now particularise for a vortex geometry. It consists of a draining bathtub flow, similar to the ones we see everyday in wash basins. Figure 2.2 shows a vortex

created at the Quantum Gravity Laboratory.

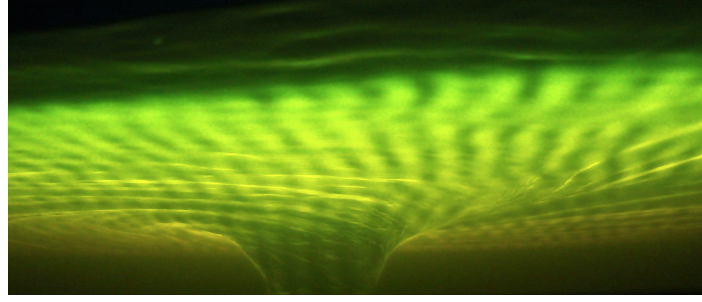


Figure 2.2: Vortex used to study the draining bathtub spacetime. Image kindly provided by The Black Hole Laboratory / Silke Weinfurtner.

The draining bathtub spacetime is best described in cylindrical coordinates. However, as the vortex is created in a very shallow container, we can, without loss of generality, work with polar coordinates on a plane – take a constant height  $z$  such that  $dz = 0$ . From now on, our choice of coordinates is  $(t, r, \theta)$ , describing a  $(1 + 2)$ -dimensional problem.

Let us determine the behaviour of the background fluid such that the vortex comes to existence. Start with the equation of continuity, which can be written as

$$\partial_t \rho + \frac{1}{r} \partial_r (r \rho v_r) + \frac{1}{r} \partial_\theta v_\theta = 0, \quad (2.23)$$

where the divergence term has been expanded. Looking at the radial derivative, we can write  $r \rho v_r = \text{constant}$ , leading to the conclusion that

$$\rho v_r \sim \frac{1}{r}. \quad (2.24)$$

The fact that the flow is vorticity free,  $\nabla \times \mathbf{v} = 0$ , also has some implications to the background velocity. Explicitly writing out the curl in cylindrical coordinates,

$$\nabla \times \mathbf{v} = \left( \frac{1}{r} \partial_\theta v_z - \partial_z v_\theta \right) \mathbf{e}_r + (\partial_z v_r - \partial_r v_z) \mathbf{e}_\theta + \frac{1}{r} (\partial_r (r v_\theta) - \partial_\theta v_r) \mathbf{e}_z, \quad (2.25)$$

one observes that only the component in  $z$  survives. The vorticity free condition dictates that

$$\partial_r (r v_\theta) - \partial_\theta v_r = 0. \quad (2.26)$$

The second term is identically zero, rendering  $r v_\theta = \text{constant}$ . Thus,

$$v_\theta \sim \frac{1}{r}. \quad (2.27)$$

Finally, conservation of angular momentum – absence of external torques – grants us one last relation. Taking into account the definition of angular momentum,

$$\mathbf{L} = \int dV \rho \mathbf{r} \times \mathbf{v}, \quad (2.28)$$

and the fact that its conservation can be expressed as  $\frac{d\mathbf{L}}{dt} = 0$ , one requires  $\rho \mathbf{r} \times \mathbf{v}$  to be constant in time. As  $\mathbf{r} = (r, 0, 0)$  and  $\mathbf{v} = (v_r, v_\theta, 0)$ , the cross product is

$$\mathbf{r} \times \mathbf{v} = \begin{vmatrix} \mathbf{e}_r & \mathbf{e}_\theta & \mathbf{e}_z \\ r & 0 & 0 \\ v_r & v_\theta & 0 \end{vmatrix} = rv_\theta \mathbf{e}_z, \quad (2.29)$$

which, in turn, implies  $\rho \mathbf{r} \times \mathbf{v} = \rho rv_\theta \mathbf{e}_z = \text{constant } \mathbf{e}_z$ . One concludes

$$\rho v_\theta \sim \frac{1}{r}. \quad (2.30)$$

From these last two constraints, we induce  $\rho$  must be constant, i.e. position independent, throughout the flow. Consequently,  $p$  and  $c$  must also be constant. The background fluid velocity can be written as

$$\mathbf{v}_0 = \frac{A\mathbf{e}_r + B\mathbf{e}_\theta}{r}, \quad (2.31)$$

with the corresponding potential  $\psi_0(r, \theta) = A \log(r/a) + B\theta$ .  $A$  and  $B$  are parameters associated to the radial and angular components of the background fluid velocity, and  $a$  is some irrelevant length scale. Observe that  $A$  can be either positive or negative:  $A < 0$  corresponds to a sink and  $A > 0$  to a source. Respectively, they will either emulate a future acoustic horizon – acoustic BH – or a past acoustic horizon – acoustic white hole.

Using equation (2.2), the acoustic metric for the draining bathtub is explicitly given by:

$$g_{\mu\nu}(t, r, \theta) = \frac{\rho}{c} \begin{pmatrix} -\left(c^2 - \frac{A^2 + B^2}{r^2}\right) & -A/r & -B \\ -A/r & 1 & 0 \\ -B & 0 & r^2 \end{pmatrix}. \quad (2.32)$$

Dropping the position independent prefactor, the line element describing the propagation of sound waves in the  $(1 + 2)$ -dimensional draining bathtub fluid flow reads

$$ds^2 = -\left(c^2 - \frac{A^2 + B^2}{r^2}\right) dt^2 - \frac{2A}{r} dt dr - 2B dt d\theta + dr^2 + r^2 d\theta^2. \quad (2.33)$$

The horizon and ergosphere of the spacetime read

$$r_H = \frac{|A|}{c} \quad (2.34)$$

$$r_e = \frac{\sqrt{A^2 + B^2}}{c}. \quad (2.35)$$

## Chapter 3

# Dynamics of Acoustic Holes

In the current chapter, we look into the dynamics of sound waves around acoustic holes. Working with the draining bathtub fluid flow, we start by assessing the behaviour of perturbations. We study under which conditions superradiance occurs, whilst examining the characteristic modes of the holes. These characteristic modes go by the name of quasinormal modes and are a very useful tool for checking the stability of the wave solutions.

### 3.1 Wave equation

In order to obtain the wave equation ruling the behaviour of sound waves in the draining bathtub flow, we recover the general result of equation (2.18) and use the background fluid flow velocity presented in equation (2.31):

$$\partial_t^2 \psi_1 + \left( \frac{A}{r} \partial_r + \frac{B}{r^2} \partial_\theta \right) \partial_t \psi_1 - \frac{c^2}{r^2} (\partial_r (r \partial_r \psi_1) + \partial_\theta^2 \psi_1) = 0. \quad (3.1)$$

The ansatz of a plane wave,

$$\psi_1(t, r, \theta) = R(r) e^{-i(\omega t - m\theta)}, \quad (3.2)$$

allows us to separate the wave equation, obtaining for the radial part

$$R_{,rr} + P_1(r) R_{,r} + Q_1(r) R = 0, \quad (3.3)$$

where

$$P_1(r) = \frac{A^2 + r^2 c^2 - 2iA(Bm - r^2 \omega)}{r(r^2 c^2 - A^2)} \quad (3.4)$$

$$Q_1(r) = \frac{2iABm + B^2 m^2 - c^2 m^2 r^2 - 2Bm\omega r^2 + r^4 \omega^2}{r^2(r^2 c^2 - A^2)}. \quad (3.5)$$

With the goal of simplifying the wave equation, one introduces the tortoise coordinate

$$\frac{dr_*}{dr} = \Delta = \left( 1 - \frac{A^2}{c^2 r^2} \right)^{-1}, \quad (3.6)$$

which explicitly reads

$$r_* = r + \frac{A}{2c} \log \left| \frac{cr - A}{cr + A} \right|. \quad (3.7)$$

This allows one to write  $R(r) = Z(r)H(r)$  and rearrange the equation so that it is expressed in terms of  $H$ :

$$Z\Delta^2 H_{,r_*r_*} + (\Delta(2Z_{,r} + P_1Z) + \Delta'Z)H_{,r_*} + (Z_{,rr} + P_1Z_{,r} + Q_1Z)H = 0. \quad (3.8)$$

By requiring  $Z$  to be a solution of the equation

$$Z_{,r} + \frac{1}{2} \frac{(c^2r^2 - A^2) + 2iA(Bm - r^2\omega)}{r(c^2r^2 - A^2)} Z = 0, \quad (3.9)$$

that is, by setting the coefficient of  $H_{,r_*}$  to zero, we reach the following Schroedinger-like wave equation:

$$H_{,r_*r_*} + \left[ c^{-2} \left( \omega - \frac{Bm}{r^2} \right)^2 - \frac{c^2r^2 - A^2}{c^2r^2} \left( r^{-2} \left( m^2 - \frac{1}{4} \right) + \frac{5A^2}{4r^4c^2} \right) \right] H = 0. \quad (3.10)$$

Using the rescaled quantities  $\hat{r} = \frac{rA}{c}$ ,  $\hat{\omega} = \frac{\omega A}{c^2}$  and  $\hat{B} = \frac{B}{A}$ , the wave equation reads

$$H_{\hat{r}_*, \hat{r}_*} + Q(\hat{r})H = 0. \quad (3.11)$$

The potential is

$$Q = \left( \hat{\omega} - \frac{\hat{B}m}{\hat{r}^2} \right)^2 - V(\hat{r}) \quad (3.12)$$

$$V = \frac{\hat{r}^2 - 1}{\hat{r}^2} \left( \hat{r}^{-2} \left( m^2 - \frac{1}{4} \right) + \frac{5}{4\hat{r}^4} \right). \quad (3.13)$$

From here onwards, all hats are dropped and one works only with the rescaled quantities. In such units, the horizon and ergosurface occur at the following radii:

$$r_H = 1, \quad r_e = \sqrt{1 + B^2}. \quad (3.14)$$

## 3.2 Wave dispersion relation

The acoustic dispersion relation of the vortex geometry may be derived by looking at the perturbation as a plane wave,

$$\psi_1 = \mathcal{A}(\mathbf{r})e^{i(\omega t - \mathbf{k} \cdot \mathbf{r})}, \quad (3.15)$$

where  $\mathbf{k} = (k, m)$  and  $\mathbf{r} = (r, \theta)$ . Using the plane wave ansatz and considering the amplitude  $\mathcal{A}(\mathbf{r})$  to be slowly varying when compared to the exponential, we obtain the following equation

$$c^2 \|\mathbf{k}\|^2 - (\omega - \mathbf{k} \cdot \mathbf{v}_0)^2 = 0, \quad (3.16)$$

which can be cast into the form of a dispersion relation:

$$\omega = \mathbf{k} \cdot \mathbf{v}_0 \pm c|\mathbf{k}|. \quad (3.17)$$

One can think of this relation as the standard dispersion relation,  $\omega = c|\mathbf{k}|$ , on a moving fluid. Indeed, the Doppler term in  $\mathbf{v}_0$  arises due to the fact that the perturbation happens on top of a moving fluid and hence its frequency shifts. The  $\pm$  sign accounts for the relative motion of the wave with respect to the motion of the background fluid. The wave may move for (+) or against (−) the background fluid.

In the specific case of the draining bathtub spacetime, the dispersion relation reads

$$\omega = \frac{Ak}{r} + \frac{Bm}{r} \pm c\sqrt{k^2 + m^2}. \quad (3.18)$$

To view how these results are affected by viscosity, cf. Reference [20].

### 3.3 Scattering in the vortex geometry. Superradiance

As previously introduced in equation (1.5), superradiance is a phenomenon that occurs when

$$\omega < mB, \quad (3.19)$$

where we have written  $B$  instead of  $\Omega$ , as  $B$  is the angular velocity at the event horizon in the draining bathtub spacetime. Now, we will show how the amplification of the incident waves comes about. In other words, one will show how the superradiant condition results in the following inequation:

$$\left| \frac{A_{\text{out}}}{A_{\text{in}}} \right|^2 > 1, \quad (3.20)$$

$A_{\text{out}}$  being the amplitude of the outgoing wave and  $A_{\text{in}}$  that of the incident wave.

Due to the complicated form of the potential in the wave equation, we cannot write an analytical solution that holds for the entire space. It must be computed numerically. Such can be achieved by imposing appropriate boundary conditions, at the horizon  $r_H = 1$  and at infinity  $r_\infty = \infty$ . In terms of the tortoise coordinate, these read  $r_{*H} = -\infty$  and  $r_{*\infty} = \infty$ . The appropriate boundary conditions correspond to the analytical solutions of the differential equation at the aforementioned radii. When  $r \rightarrow r_H$ ,  $V \rightarrow 0$  and  $Q \rightarrow (\omega - Bm)^2$ , yielding

$$H_{r_*, r_*} + (\omega - Bm)^2 H = 0. \quad (3.21)$$

The solutions of the differential equation are of the form  $H \sim e^{\pm i(\omega - Bm)r_*}$ , where our convention of time dependency dictates that the minus sign corresponds to incoming waves and the plus sign to outgoing waves. Given the nature of the horizon, which is, by definition, the geometrical place from which no information comes out, we require there to be only incoming waves. The solution at the sonic horizon

then reads

$$H_H = A_H e^{-i(\omega - Bm)r_*}. \quad (3.22)$$

For sufficiently large radius, when  $V \rightarrow 0$  and  $Q \rightarrow \omega^2$ , the wave equation reads

$$H_{r_*, r_*} + \omega^2 H = 0, \quad (3.23)$$

which yields the solution

$$H_\infty = A_{\text{in}} e^{-i\omega r_*} + A_{\text{out}} e^{i\omega r_*}. \quad (3.24)$$

In a wrap, we use the solutions at the horizon, equation (3.22), and at infinity, equation (3.24), as boundary conditions for the numerical solution of the wave equation.

Now that we have properly motivated the need for boundary conditions, and derived them, we return to the initial argument that superradiance results in the amplification of incident waves. We start by rewriting the boundary conditions as

$$H_\infty = R_{\omega m} e^{i\omega r_*} + e^{-i\omega r_*} \quad (3.25)$$

$$H_H = T_{\omega m} e^{-i(\omega - mB)r_*}, \quad (3.26)$$

where  $R_{\omega m}$  is the reflection coefficient and  $T_{\omega m}$  the transmission coefficient. Note that normalisation of the incoming wave has been assumed, as we have set its amplitude to 1 in equation (3.25). It has been made evident that both the reflection and transmission coefficients depend on the wave frequency  $\omega$  and on the azimuthal number  $m$ . Observe the reflection coefficient is defined as

$$|R_{\omega m}|^2 = \left| \frac{A_{\text{out}}}{A_{\text{in}}} \right|^2, \quad (3.27)$$

as it tells us about the component of the wave that is reflected back in a scattering experiment. The transmission coefficient, on the other hand, refers to the component of the wave that is transmitted through the scattering surface. These components beg for an energy conservation equation. In standard potential step scattering problems, such conservation equation is of the form

$$1 - |R|^2 = |T|^2, \quad (3.28)$$

$|R|^2$  and  $|T|^2$  generic reflection and transmission coefficients, respectively. Observe the energy conservation condition is very intuitive, as it claims the energy carried by the wave before and after scattering must match; read  $1 = |T|^2 + |R|^2$ , with the LHS referring to the energy before scattering and the RHS to the one after scattering. The aim of the following calculations is to deduce a similar equation. Such can be achieved by realising the wave equation of our problem does not have any dependencies on  $H_{,r_*}$ . When this happens, the Wronskian is constant in the variable  $r_*$ . Proof of this statement can be found

in Section 5.3. The Wronskian  $W$  of two given functions  $y_1(r)$  and  $y_2(r)$  is defined as

$$W(y_1, y_2) = \begin{vmatrix} y_1 & y_2^\dagger \\ y_1' & y_2'^\dagger \end{vmatrix}. \quad (3.29)$$

So now it is just a matter of computing the Wronskian of the solutions  $H$  and  $H^\dagger$  at the event horizon and at infinity,

$$W_\infty(H, H^\dagger) = 2i\omega (1 - |R_{\omega m}|^2) \quad (3.30)$$

$$W_H(H, H^\dagger) = 2i(\omega - Bm)|T_{\omega m}|^2, \quad (3.31)$$

and equating them

$$1 - |R_{\omega m}|^2 = \left(1 - \frac{Bm}{\omega}\right) |T_{\omega m}|^2. \quad (3.32)$$

It has become evident that in superradiant regimes the reflection coefficient must be greater than 1. That is, equation (3.20) is verified.

Next, we work with the wave equation

$$\left(1 - \frac{1}{r^2}\right)^2 \frac{d^2 H}{dr^2} + \frac{2}{r^3} \left(1 - \frac{1}{r^2}\right) \frac{dH}{dr} + Q(r)H = 0, \quad (3.33)$$

where we have written the derivatives with respect to the tortoise coordinate  $r_*$  in terms of the radial coordinate  $r$ . Recall the definition of the potential,

$$Q(r) = \left(\omega - \frac{Bm}{r^2}\right)^2 - \frac{r^2 - 1}{r^2} \left(\frac{1}{r^2} \left(m^2 - \frac{1}{4}\right) + \frac{5}{4r^4}\right).$$

The numerical method used to solve the wave equation consists in iteratively integrating it for different frequencies  $\omega$ , imposing the boundary conditions of equations (3.22) and (3.24). The output of each cycle consist of a pair of points  $(\omega, |R_{\omega m}|^2)$ , which is later plotted. A series expansion with the aim of increasing precision near the boundaries is performed – see equations (3.36) and (3.37) for an illustrative example. We normalise the incoming wave by setting  $A_H = 1$  in equation (3.22).

In Figure 3.1, we present some of the plots produced. In the plots, we have included a dashed line at  $|R_{\omega m}|^2 = 1$ . This line sets the frontier between the cases of no amplification and amplification. Whenever the curves are above the dashed line, there is superradiant scattering. It is interesting to note that the intersection of each curve with the horizontal line happens when  $\omega = mB$ , as predicted by the theory. Out of the parameters chosen, the maximum value obtained for amplification was  $|R_{\omega m}|^2 = 1.805$  for  $\omega = 4.18$ ,  $m = 1$  and  $B = 5$ . Larger amplification is obtained for larger values of the rotation parameter  $B$ . Once rotation is the source of amplification in superresonant mechanisms, it is natural that the greater the rotational speed, the greater the amplification: more rotational energy is available. This very same reason justifies that  $B = 0$  produces no amplification. We also see that greater amplification occurs for  $m = 1$  rather than for  $m = 2$ . An explanation for this phenomenon is discussed in Appendix A. The results obtained are consistent with previous works, in particular with Figure 2 in Reference [21].

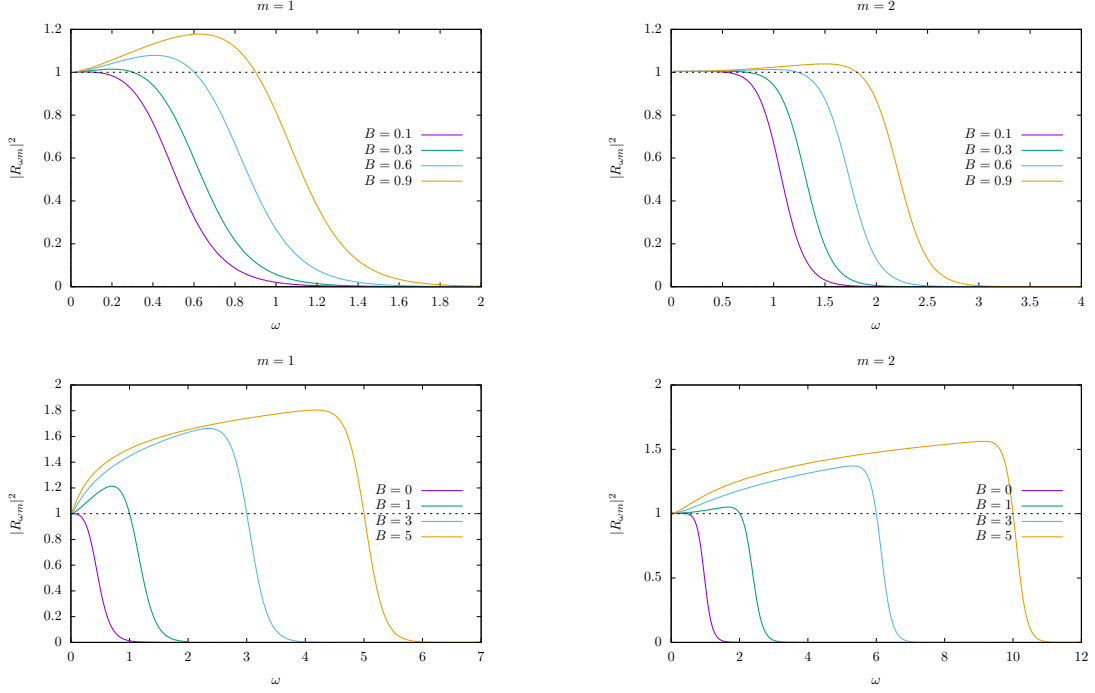


Figure 3.1: Reflection coefficient  $|R_{\omega m}|^2$  as a function of  $\omega$ . Several solutions for the differential equation are produced, as one changes the value of parameter  $B$ , the angular velocity at the horizon. The left hand panels show the results for  $m = 1$  and the right hand ones the results for  $m = 2$ .  $|R_{\omega m}|^2 = 1$  (limit above which superradiance occurs) is plotted as a dashed line.

One observes the reflection factor is never larger than 2. This upper bound is also present in the Reissner–Nordstroem BH and as we will see in the cylindrical setup evaluated in the following chapters. We refer to an explanation for such factor then.

### 3.4 Quasinormal modes and stability

Working with the boundary conditions presented in Section 3.3, we now turn our analysis to the Quasinormal Modes (QNMs) of the  $(1 + 2)$ -dimensional bathtub flow. If an isolated guitar string vibrates in normal modes, a guitar string coupled to air vibrates in QNMs. In fact, the energy transfer occurring from the string to the surrounding air adds on an imaginary part to the frequency of the (quasi)normal modes. This imaginary part directly accounts for the losses or, in the opposite range of the spectrum, for instabilities associated to wave amplification.

In order to properly assess the behaviour of the wave equation, we look at the radial time-dependent solution at infinity,  $\Psi \sim e^{ikr - i\omega t}$ , which can be rewritten as

$$\Psi \sim e^{i\omega(r-t)} \quad (3.34)$$

when natural units ( $c = 1$ ) are considered. The particular solution considered in equation (3.34) corresponds to the outgoing part of the wave, in accordance with the boundary conditions imposed of no incoming waves at infinity. Note that an analogous analysis for  $\Psi \sim e^{-ikr + i\omega t}$  (incoming solutions) could

also be considered. A complex frequency  $\omega = \omega_R + i\omega_I$  leads to solutions

$$\Psi \sim e^{i\omega_R(r-t)} e^{-\omega_I(r-t)}, \quad (3.35)$$

where  $\omega_R$  influences the phase of the wave and  $\omega_I$  modifies its amplitude. Moreover, the sign of  $\omega_I$  determines the stability of the solution:

- $\omega_I > 0$      Damped solution in space, unstable (amplified) in time.
- $\omega_I < 0$      Amplified solution in space, stable (damped) in time.

In order to compute the QNMs, we use direct integration a la Chandrasekhar-Detweiler [22]. The gist of the method is illustrated in Figure 3.2.

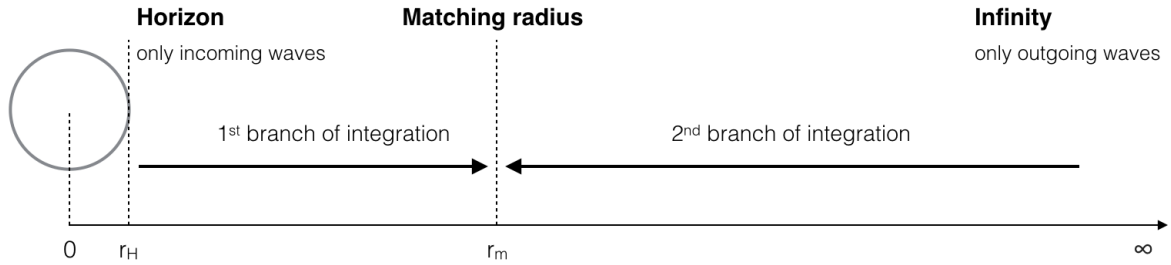


Figure 3.2: Gist of the numerical method of direct integration used to compute the QNMs. We consider two integrations, the first being from  $r_H$  to  $r_m$  and the second from  $r_m$  to  $\infty$  (more accurately, to numerical infinity). At  $r_m$  (matching radius), both solutions and their respective derivatives must match.

Working towards the increase in precision in the numerical integrations, we define series that are ansatz for solutions in the regions of interest. Particularly, at the horizon and at infinity. The series ansatz are

$$\text{Horizon:} \quad H_h = (r-1)^{-i(\omega-mB)/2} \sum_{n=0}^{\infty} h_n (r-1)^n \quad (3.36)$$

$$\text{Infinity:} \quad H_\infty = e^{i\omega r} \sum_{n=0}^{\infty} \frac{g_n}{r^n}, \quad (3.37)$$

where the coefficients  $h_n$  and  $g_n$  are computed numerically, by matching the ansatz with the wave equation. For a generic frequency, the wave equation is continuous but its derivative is discontinuous at the matching point. On the other hand, frequencies corresponding to QNMs produce functions with continuous derivative. Finally, one should note that the frequency of the QNMs should not depend on the matching radius  $r_m$  chosen. Taking these requirements into account, one arrives at the QNM frequencies displayed in Table 3.1. The results are in accordance with the existing literature, namely with References [21] and [23]. Bearing in mind the stability arguments presented above, one concludes that no instabilities arise in the QNMs discovered, as  $\omega_I < 0$ .

$m$	$\omega_{\text{QNM}}$
1	$0.4069 - 0.3412i$
2	$0.9527 - 0.3507i$
3	$1.4685 - 0.3524i$
4	$1.9765 - 0.3530i$

Table 3.1: Fundamental quasinormal frequencies, for  $B = 0$ .

## Chapter 4

# Dynamics of Acoustic Geometries

The vortex geometry presented before, despite being very elegantly formulated, is rather troublesome to the experimentalist. At supersonic velocities, effects such as turbulence may arise. This is greatly inconvenient as these effects spoil the analogue model described previously. In the present chapter, we analyse another experimental setup that does not require supersonic velocities. Such setup relies on the existence of a rotating cylinder as a possible source of amplification. Firstly, we assess how the sound waves interact with the rotating cylinder in a scattering experiment. We wish to investigate whether the existence of horizons is a requirement for superradiance. Furthermore, with the aim of studying superradiant instabilities, we add another cylinder, concentric with the first one and of larger radius. In a superradiant regime, we expect to see a sequential amplification of the waves, reflection after reflection, as a result of the confinement.

### 4.1 Wave equation

The new setup consists of fluid surrounding a rotating cylinder. We consider the fluid to be at rest, despite the rotation of the cylinder. As we previously saw, the most general wave equation ruled by the continuity and the Euler equations is expressed by equation (2.18). When we take into account a static fluid configuration,  $\mathbf{v}_0 = 0$ , such wave equation simply becomes

$$\partial_t^2 \psi_1 - \nabla \cdot (c^2 \nabla \psi_1) = 0. \quad (4.1)$$

Using the plane wave equation ansatz given by equation (3.2), where we identify  $R(r) = \frac{\varphi(r)}{\sqrt{r}}$ ,

$$\psi(t, r, \theta) = \frac{\varphi(r)}{\sqrt{r}} e^{-i(\omega t - m\theta)}, \quad (4.2)$$

the wave equation (4.1) becomes

$$\partial_r^2 \varphi + \left( \frac{\omega^2}{c^2} - \frac{1}{r^2} \left( m^2 - \frac{1}{4} \right) \right) \varphi = 0. \quad (4.3)$$

This wave equation has a known analytical solution, expressed in terms of the Bessel functions,

$$\varphi(r) = D_1 \sqrt{r} J_m(\omega r/c) + D_2 \sqrt{r} Y_m(\omega r/c), \quad (4.4)$$

where  $D_1$  and  $D_2$  are constants to be determined according to boundary conditions.

## 4.2 Scattering off a rotating cylinder. Superradiance

The cylinder, of radius  $R_0$ , is characterised by a quantity called acoustic impedance. Its value determines the interaction wall-fluid. The acoustic impedance  $Z$ , as defined in Reference [24], is

$$Z(\mathbf{x}, \omega) = \frac{p(\mathbf{x}, \omega)}{\mathbf{v}(\mathbf{x}, \omega) \cdot \mathbf{n}_s(\mathbf{x})}, \quad (4.5)$$

where  $p$  and  $\mathbf{v}$  are respectively the pressure and velocity of the fluid,  $\mathbf{n}_s$  is the normal to the surface on which the velocity is measured,  $\omega$  is the wave frequency and  $\mathbf{x}$  refers to the position at which the aforementioned quantities are evaluated. Note that the impedance is a complex variable. The real part is called resistance and the imaginary part is the reactance. The concept of the resistance is similar to that of a regular resistance. Think in terms of Ohm's law. A given material, depending on its resistance, will dissipate more or less energy. The reactance, on the other hand, measures the dephasing of the sound wave during the interaction.

Under the conditions described in Reference [14],  $Z_\omega$  can be written as

$$\left( \frac{\partial_r \psi_1}{\psi_1} \right) \Big|_{r=R_0} = -\frac{i\rho_0\omega}{Z_\omega}. \quad (4.6)$$

This definition stems from the barotropic condition, where the pressure can be expressed as  $p_1 = -\rho_0 \partial_t \psi_1 = -i\omega\rho_0\psi_1$ . In terms of the radial field defined via equation (4.2), equation (4.6) reads

$$\partial_r \varphi = \left( -\frac{i\rho_0\omega}{Z_\omega} + \frac{1}{2R_0} \right) \varphi \Big|_{r=R_0}. \quad (4.7)$$

This equation is the boundary condition one imposes at  $r = R_0$ . For a cylinder rotating uniformly with angular velocity  $\Omega$ , the frequency of the incident wave can be modified to include the angular rotation such that

$$\omega \rightarrow \tilde{\omega} = \omega - m\Omega. \quad (4.8)$$

One can arrive at a condition for energy conservation using equation (4.7) as a tool to compute the Wronskian at  $R_0$ ,

$$W_{R_0}(\varphi, \varphi^\dagger) = 2i\rho_0\tilde{\omega} \frac{\text{Re}(Z_{\tilde{\omega}})}{|Z_{\tilde{\omega}}|^2} |\varphi(R_0)|^2. \quad (4.9)$$

In the limit  $r \rightarrow \infty$ , the wave equation (4.1) behaves as equation (3.24). Recall the latter described the wave solution at infinity for the vortex spacetime. As a result, the Wronskian of both wave equations is the same. Once again, the radial wave equation does not depend on the first order derivative in  $r$  of the

field. We equate  $W_{R_0}(\varphi, \varphi^\dagger)$  with  $W_\infty(\varphi, \varphi^\dagger)$ ,

$$1 - |R_{\omega m}|^2 = \left(1 - \frac{m\Omega}{\omega}\right) \rho_0 \frac{\text{Re}(Z_{\bar{\omega}})}{|Z_{\bar{\omega}}|^2} |\varphi(R_0)|^2. \quad (4.10)$$

Also in the cylinder spacetime the superradiance condition  $\omega < m\Omega$  implies  $|R_{\omega m}|^2 > 1$ .

Similarly to what we did in the previous chapter, when studying scattering and superradiance, we present here the output of the reflection coefficient as a function of the frequency  $\omega$  of the perturbed sound waves. The numerical implementation is in all identical to the previous one. A very obvious distinction between the curves in the two spacetimes has to do with the fact that here the curve never reaches  $|R_{\omega m}|^2 = 0$ . This is a consequence of the definition of the acoustic impedance, which has been set to  $Z = 1 - i$ . This value is standard for several known materials [25]. Out of the plots displayed, the

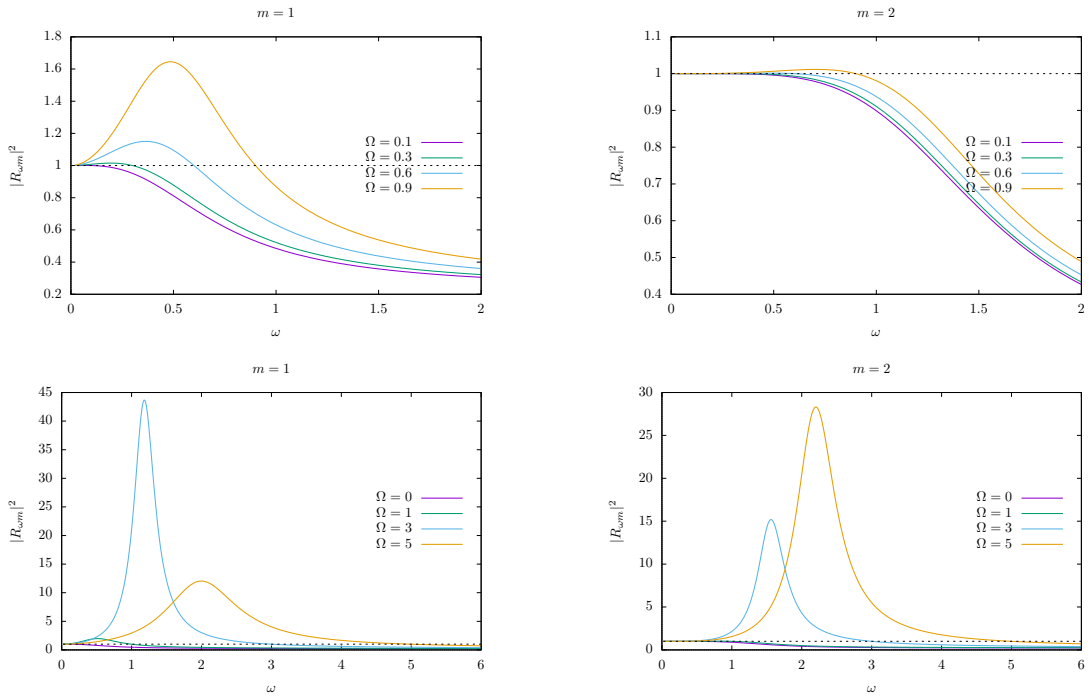


Figure 4.1: Reflection coefficient  $|R_{\omega m}|^2$  as a function of  $\omega$ . Several solutions for the differential equation are produced, as one changes the value of parameter  $\Omega$ , the angular velocity of the rotating cylinder. The left hand panels show the results for  $m = 1$  and the right hand ones the results for  $m = 2$ .  $|R_{\omega m}|^2 = 1$  (limit above which superradiance occurs) is plotted as a dashed line. The following parameters were used:  $c = \rho_0 = R_0 = 1$  and  $Z = 1 - i$ .  $\Omega$  is presented in units of  $c/R_0$ .

maximum amplification for  $m = 1$  occurs when  $\Omega = 3$  and it corresponds to  $|R_{\omega m}|^2 = 43.677$ , at  $\omega = 1.18$ . For  $m = 2$ , we recognise the maximum amplification happens when  $\Omega = 5$ , with  $|R_{\omega m}|^2 = 28.314$ , at  $\omega = 2.20$ . The location of the maxima is related to the QNMs. We address this issue in Section 4.3.

An interesting exercise would be to determine the optimal conditions for amplification. For  $m = 1$  and  $m = 2$ , we find the rotational speed  $\Omega$  for which the amplification of the perturbations is the greatest. In order to do that, we reproduce the curves above for a larger set of values of  $\Omega$ . At each of those values, we assess the maximum amplification. The results obtained are given in Table 4.1. Note the maximum amplification associated to  $m = 1$  is greater than the one to  $m = 2$ , as usual. Finally, one should mention that when  $\Omega = 0$ , the curve is always below the dashed  $|R_{\omega m}|^2 = 1$  line. In other words,

	$m = 1$	$m = 2$
$\Omega$	2.3	3.8
$ R_{\omega m} ^2$	4990.6	1497.4
$\omega$	0.91	1.81

Table 4.1:  $\Omega$  that maximises the reflection coefficient  $|R_{\omega m}|^2$  for  $m = 1$  and  $m = 2$ .  $\Omega$  is in units of  $c/R_0$ .

when the cylinder is not rotating, there is no amplification. Indeed, a non-rotating cylinder is a cylinder from which no energy can be extracted.

The amplification is never larger than  $|R_{\omega m}|^2 = 2$  when  $\Omega < 1$ . This behaviour is displayed in Figure 4.2, where we zoom in the region corresponding to superradiance for rotational speeds  $\Omega < 1$ . Using WKB expansions, one can predict such limit. For a full discussion on the subject cf. Reference [26].

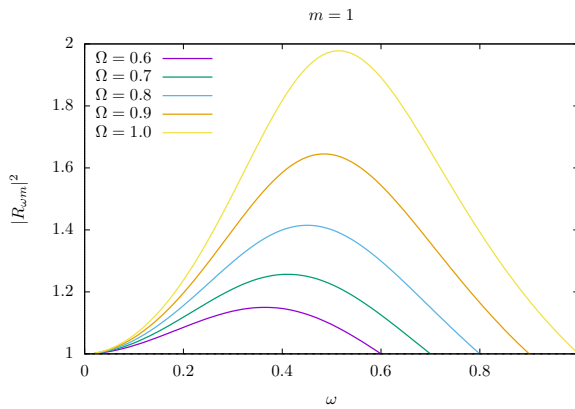


Figure 4.2: Reflection coefficient  $|R_{\omega m}|^2$  as a function of  $\omega$ . We zoom in the region for which superradiance occurs, plotting the results for  $\Omega \leq 1$ . One observes the amplification is increasing with  $\Omega$ , but never reaching  $|R_{\omega m}|^2 = 2$ .  $\Omega$  is in units of  $c/R_0$ .

When we exit the realistic range of values for the acoustic impedance, we observe the upper bound of 2 no longer exists. We refer to Figure 4.3 to illustrate such behaviour, where  $Z$  has been set to one tenth of its real value. On the other hand, larger values of acoustic impedance yield smaller values of

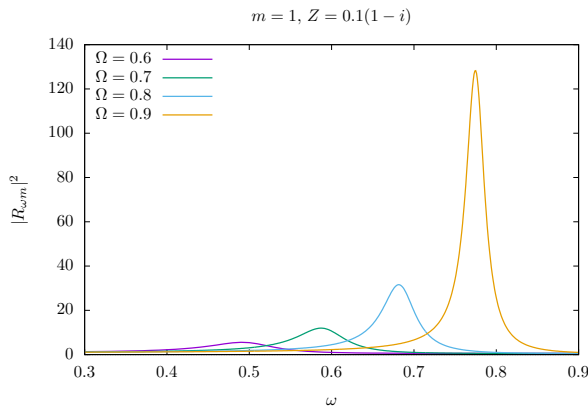


Figure 4.3: Reflection coefficient  $|R_{\omega m}|^2$  as a function of  $\omega$ . We look at smaller values of the acoustic impedance to conclude that they allow for greater amplification. When  $Z = 0.1(1 - i)$ , the upper bound of  $|R_{\omega m}|^2 = 2$  no longer exists.  $\Omega$  is in units of  $c/R_0$ .

amplification, as demonstrated by Figure 4.4. There is a tendency that larger impedances return smaller

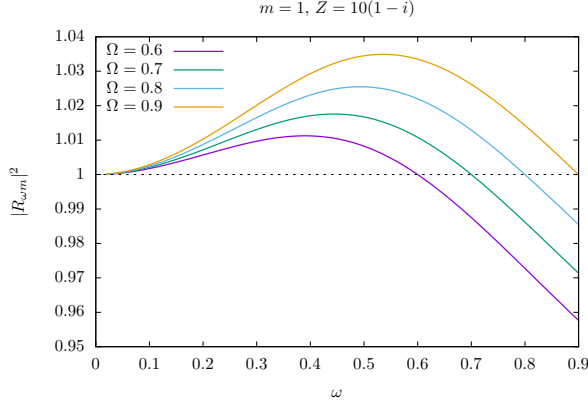


Figure 4.4: Reflection coefficient  $|R_{\omega m}|^2$  as a function of  $\omega$ . We look at greater values of the acoustic impedance,  $Z = 10(1 - i)$ , to conclude that they yield lower amplification values.  $\Omega$  is in units of  $c/R_0$ .

amplifications; and vice-versa. This result makes sense when we think of the nature of impedance, which is that of a resistance – the imaginary part of the impedance will only influence the phase of the reflected wave, so we need not worry about it for the current discussion. The resistance dictates how much of the energy carried by the incoming wave is lost at the boundary. Hence, the greater the resistance, the greater the energy loss at the cylinder wall. Consequently, we expect to see a decrease in the reflection coefficient. See Figure 4.5, where we plot different values of  $Z$  for a fixed rotational speed  $\Omega = 0.7 c/R_0$ .

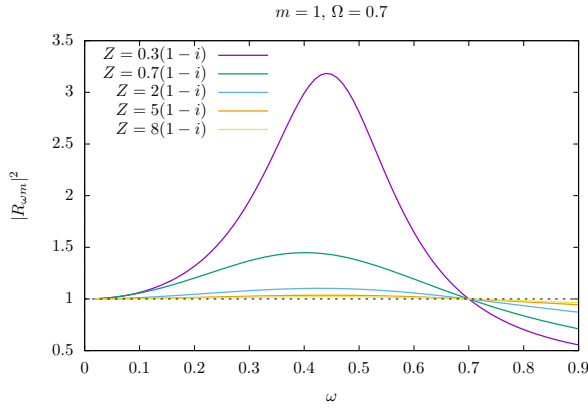


Figure 4.5: Reflection coefficient  $|R_{\omega m}|^2$  as a function of  $\omega$ . By keeping the rotation speed of the cylinder constant ( $\Omega = 0.7 c/R_0$ ), we see how different acoustic impedances influence the reflection coefficient. One can clearly observe that the smaller the impedance, the larger the amplification. Finally, it is interesting to note the superradiant regime ceases to exist as soon as  $\omega$  reaches 0.7, as predicted by the superradiance condition ( $m\Omega = 0.7$ ).

### 4.3 Quasinormal modes and stability

In the spirit of studying superradiance-triggered instabilities, we look at the QNMs of the system. We will do this in a slightly different fashion than before. By confining the cylinder, we look at solutions whose frequencies  $\omega$  are invariant under changes of such confinement radius. The confinement is achieved by

adding a cylinder to our setup. It has radius  $R_1 > R_0$  and is concentric with the first one, as displayed in Figure 4.6. We impose the outer cylinder to behave as a perfect mirror. That is, the outer wall reflects

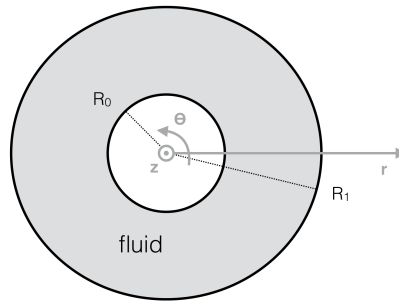


Figure 4.6: Pictorial view of the confined setup.

back all incident radiation. The boundary condition at  $R_1$ , defined in terms of the radial velocity, reads

$$\mathbf{v}_1 \cdot \mathbf{e}_r = 0 \implies \partial_r \psi_1 = 0, \quad (4.11)$$

which, in terms of the radial field, corresponds to setting

$$\partial_r \varphi - \frac{\varphi}{2r} = 0. \quad (4.12)$$

This boundary condition could as easily been derived by setting  $Z_\omega \rightarrow \infty$  in equation (4.6). Note that a material with an infinitely large acoustic impedance is one that forbids any radiation to go through, resulting in total reflection of the wave.

In this configuration, whenever both  $\omega_R$  and  $\omega_I$  are constant, we have found a QNM. In Figure 4.7, the solutions for rotational speeds  $\Omega$  of 5, 4 and 3 are QNMs. The remaining, despite having a constant  $\omega_I$  for high values of  $R_1/R_0$ , have a varying  $\omega_R$  and thus are not QNMs of the open system. The

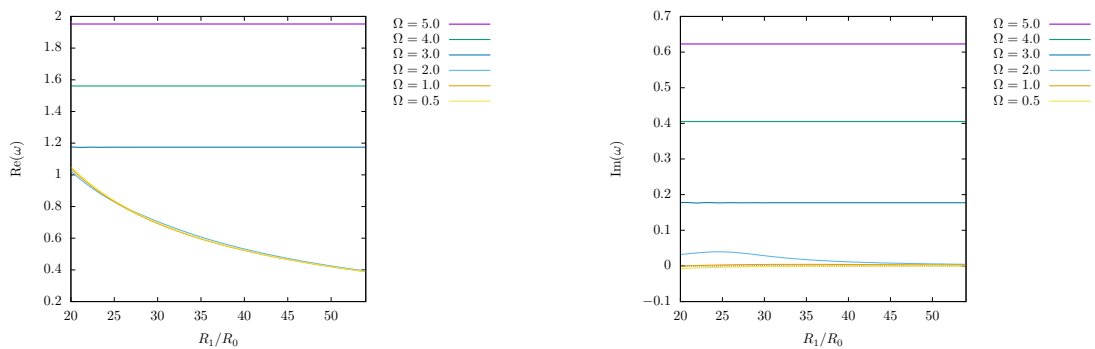


Figure 4.7: Real and imaginary parts of the frequency  $\omega$  as functions of the confinement radius  $R_1/R_0$ . If  $\omega$  remains constant as the radius changes, eliminating the outer wall altogether will produce no change in the frequency. Frequencies in such a regime are those of QNMs.  $\Omega$  is in units of  $c/R_0$ .

requirement for constancy of  $\omega$  ensures the frequency at infinity to be the same as the one found in the confined setup. In fact, the QNMs found are frequencies which solve the wave equation (4.3) for a given radius  $R_1 > R_0$ . Notice that  $R_1$  corresponds to the upper radius of integration in the numerical implementation of the problem. Physically, we can think of an outer cylinder with an increasingly larger

radius, producing the same wave solutions. Make such radius large enough ( $R_1 \rightarrow \infty$ ) and one has found the characteristic frequency of the open system, the QNM. These are listed in Table 4.2.

$\Omega$	$\omega_{\text{QNM}} (m = 1)$	$\omega_{\text{QNM}} (m = 2)$
3.0	$1.1744 + 0.1772i$	–
3.5	$1.3669 + 0.2928i$	–
4.0	$1.5610 + 0.4050i$	–
4.5	$1.7562 + 0.5148i$	$2.0124 + 0.1912i$
5.0	$1.9522 + 0.6228i$	$2.1845 + 0.3262i$
5.5	$2.1487 + 0.7295i$	$2.3618 + 0.4564i$
6.0	$2.3457 + 0.8351i$	$2.5428 + 0.5825i$

Table 4.2: Frequencies of QNMs, for  $m = 1$  and  $m = 2$ . The frequencies presented correspond to the fundamental mode. The entries of the table marked with – are those for which we could not find the corresponding  $\omega_{\text{QNM}}$ . We were able to find QNM down to  $\Omega = 2.8$  for  $m = 1$  and  $\Omega = 4.2$  for  $m = 2$ .

Recall the discussion in Section 3.4; the QNMs displayed are unstable ( $\omega_I > 0$ ). The result is not surprising. The frequencies of Table 4.2 correspond to domains where superradiance is present – cf. Figure 4.1. Unstable frequencies result in wave amplification, which is precisely the definition of superradiance. Hence, we arrive at a very handy rule of thumb: whenever the QNMs are given by frequencies whose imaginary part is positive, we are in the presence of superradiance; the reverse implication is also true. Note this justifies the fact that the QNMs in Section 3.4 are stable. They were computed for  $B = 0$ , where superradiance does not exist.

Comparing the QNM frequencies displayed in Table 4.2 with Figure 4.1, one identifies a correspondence between the maximum amplification and the location of the QNMs. See Figure 4.8, where we have plotted the  $|R_{\omega m}|^2$  curves, signalling the QNM frequencies as well. A QNM is, by definition, a mode

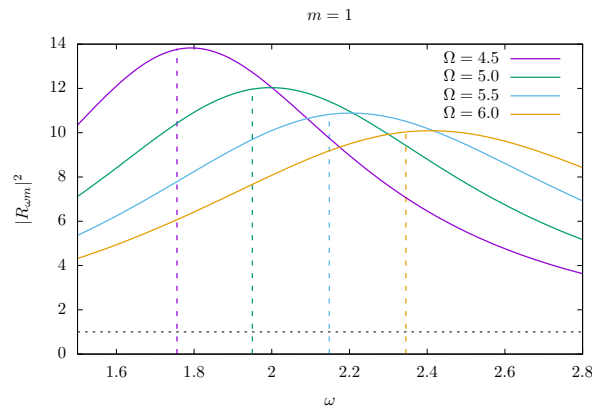


Figure 4.8: Reflection coefficient  $|R_{\omega m}|^2$  as a function of  $\omega$ . We focus our analysis in the relation between the maximum amplification factor and  $\omega_{\text{QNM}}$  by drawing vertical lines that correspond to  $\text{Re}(\omega_{\text{QNM}})$ . The QNMs are drawn in the same colour as the respective reflection curves.  $\Omega$  is in units of  $c/R_0$ .

in which the wave is described by

$$\psi = A_{\text{out}} e^{-i\omega_{\text{QNM}} r}, \quad r \rightarrow \infty. \quad (4.13)$$

This is a solution where  $A_{\text{in}} = 0$ . Hence, in this regime, we expect  $|R_{\omega m}|^2 \rightarrow \infty$ . If we were dealing with

normal modes (with purely real frequencies), we would expect the reflection coefficient to be roughly described by  $\delta(\omega - \omega_{\text{QNM}})$ . That is, the maximum amplification would occur for  $\omega = \omega_{\text{QNM}}$ . However, the presence of an imaginary frequency shapes the Dirac delta into a Gaussian, rendering the maximum amplification close to  $\text{Re}(\omega_{\text{QNM}})$ , but not precisely there.

Yet an additional approach to this problem consists in investigating whether the QNMs and  $\Omega$  are related. With that in mind, we looked at other values of  $\Omega$  and searched for the corresponding  $\omega_{\text{QNM}}$ . The results are in Figure 4.9. The data was adjusted to a linear regression  $\omega_{\text{QNM}} = a\Omega + b$ . The fit

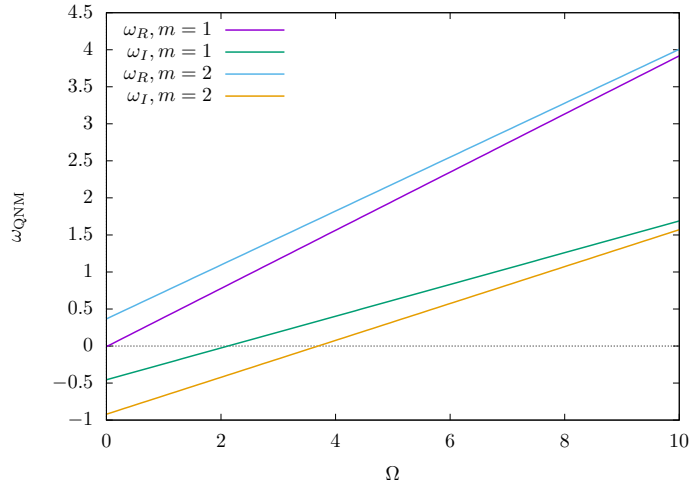


Figure 4.9: Linear regressions for the values of frequency of the QNMs, real and imaginary. Two sets of regressions are displayed, corresponding to results for  $m = 1$  and  $m = 2$ .  $\Omega$  is in units of  $c/R_0$ .

parameters are in Table 4.3. These regressions have a domain of validity, having been confirmed up

	$m = 1$		$m = 2$	
	$\omega_R$	$\omega_I$	$\omega_R$	$\omega_I$
$a$	$0.3926 \pm 0.0002$	$0.2144 \pm 0.0005$	$0.3640 \pm 0.0010$	$0.2491 \pm 0.0011$
$b$	$-0.0083 \pm 0.0013$	$-0.4554 \pm 0.0028$	$0.3663 \pm 0.0062$	$-0.9206 \pm 0.0070$

Table 4.3: Fit parameters for the plots displayed in Figure 4.9. The linear fit equation is  $\omega_{\text{QNM}} = a\Omega + b$ .

until  $\Omega \sim 33 c/R_0$  for  $m = 1$  and  $\Omega \sim 10 c/R_0$  for  $m = 2$ .

## 4.4 Confined geometry

Rather than using the confinement as a means of computing QNMs, one examines how it can impact the stability of the solutions. We turn our attention to the values of  $\omega_I$  in subcritical rotational speeds:  $\Omega < c/R_0$ . A close look at Figure 4.7 and we see that, as one approaches subsound rotational speeds,  $\omega_I$  becomes smaller and smaller. At a certain point, it may even become negative. In fact, for some rotational speeds  $\Omega$  and at given ratios  $R_1/R_0$ , there are stable solutions ( $\omega_I < 0$ ). The behaviour is displayed in Figure 4.10.

The data there seems to suggest that for increasingly lower rotational speeds, the point where the curve for  $\omega_I(R_1/R_0)$  crosses the  $\omega = 0$  axis is increasingly higher. Working with other values of  $\Omega$  and

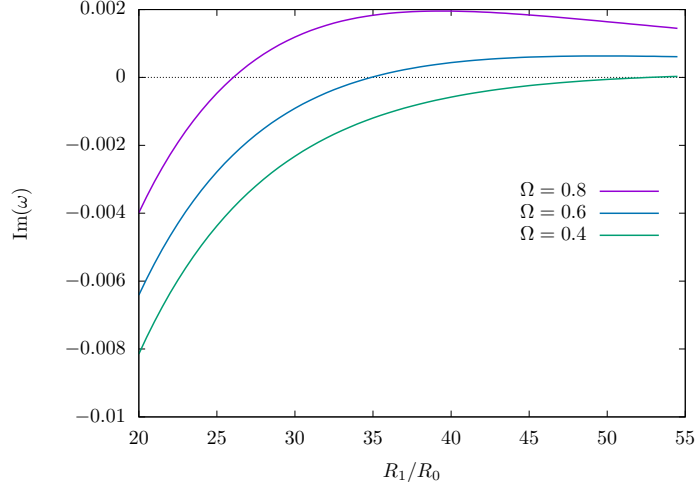


Figure 4.10: Imaginary part of the frequency versus the radius  $R_1/R_0$ . For subcritical values of  $\Omega$ , one can find stable solutions at certain ratios  $R_1/R_0$ .  $\Omega$  is in units of  $c/R_0$ .

studying where this crossing occurs, we produce the results of Figure 4.11, which fit to  $R_1/R_0 = \frac{a}{\Omega}$ .  $a$  is a free parameter. Note that we have some results for  $\Omega > 1$ . In that domain, the crossing is also present. We had not noticed it in Figure 4.7, as it happens outside the range of  $R_1/R_0$  considered. To decode the

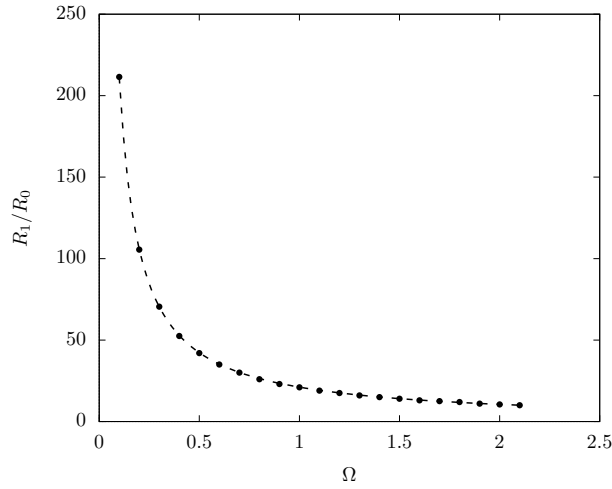


Figure 4.11: Coordinates  $R_1/R_0$  and  $\Omega$  for which  $\omega_I = 0$ . For increasingly lower rotational speeds, the point where the curve for  $\omega_I(R_1/R_0)$  crosses the  $\omega = 0$  axis is increasingly higher. The fit equation is  $R_1/R_0 = (21.1154 \pm 0.0175)/\Omega$ .

nature of the fit, we can think of the physical consequences of setting  $\omega_I = 0$ . In the limit of vanishing  $\omega_I$ , superradiant instabilities are non-existing. More precisely, we are in the regime where  $\omega = m\Omega$ ,  $\omega$  being a purely real frequency. Our knowledge of normal modes allows us to recognise that, given finite boundary conditions,  $\omega$  is inversely proportional to the distance between such finite boundaries. In our specific case, we can thus write

$$\frac{1}{R_1/R_0} \sim m\Omega, \quad (4.14)$$

in agreement with the numerical results.



## Chapter 5

# Dynamics of Acoustic Geometries in Viscous Flows

In the current chapter we inspect the behaviour of acoustic perturbations in viscous fluids. In particular, we hope to validate our approach of working with water, considering it to be non-viscous. If we cannot do so, we wish to see how good of an approximation it is. We start by presenting the modifications to the governing equations and deriving the corresponding wave equation. Then, we explore how viscosity alters the results in scattering experiments as well as the QNMs of the system.

### 5.1 Governing equations and wave equation

Viscosity is a phenomenon of internal friction, which causes an irreversible transfer of momentum from points where the velocity is large to those where it is small. Processes of internal friction occur in a fluid only when different fluid particles move with different velocities, so that there is a relative motion between various parts of the fluid. Including viscosity in the treatment done so far means that a modification of the fluid equations is in order. At this point, we substitute the Euler equation by the Navier-Stokes equation,

$$\rho \partial_t \mathbf{v} + \rho \mathbf{v} \cdot \nabla \mathbf{v} = -\nabla p + \mu \nabla^2 \mathbf{v} + \left( \xi + \frac{\mu}{3} \right) \nabla (\nabla \cdot \mathbf{v}). \quad (5.1)$$

This formulation of the Navier-Stokes equation holds for compressible flows, where we require  $\mu$  and  $\xi$  to be constant throughout the flow.  $\mu$  and  $\xi$  are, respectively, the dynamic and second (bulk) viscosities of the fluid. The following vector identities

$$\nabla^2 \mathbf{v} = \nabla (\nabla \cdot \mathbf{v}) - \nabla \times (\nabla \times \mathbf{v}) \quad (5.2)$$

$$\mathbf{v} \cdot \nabla \mathbf{v} = \frac{1}{2} \nabla v^2 + (\nabla \times \mathbf{v}) \times \mathbf{v}, \quad (5.3)$$

may be used to simplify the equation. Taking into account the fact that the flow is irrotational,  $\nabla \times \mathbf{v} = 0$ , equation (5.1) further simplifies to

$$\partial_t \mathbf{v} = -\frac{1}{2} \nabla v^2 - \frac{\nabla p}{\rho} + \frac{\alpha}{\rho} \nabla^2 \mathbf{v}, \quad (5.4)$$

where  $\alpha$ , the viscosity parameter, is defined as  $\alpha = \xi + \frac{4}{3}\mu$ . Linearising and following the procedure described in Section 2.1, we obtain the perturbed version of the Navier-Stokes equation,

$$\partial_t \nabla \psi_1 = -\nabla(\nabla \psi_0 \nabla \psi_1) - \frac{\nabla p_1}{\rho_0} + \frac{\alpha}{\rho_0} \left( \nabla^2(\nabla \psi_1) - \frac{\rho_1}{\rho_0} \nabla^2(\nabla \psi_0) \right), \quad (5.5)$$

which can be integrated out and rewritten as

$$\partial_t \psi_1 = -\mathbf{v}_0 \cdot \nabla \psi_1 - \frac{p_1}{\rho_0} + \frac{\alpha}{\rho_0} \left( \nabla^2 \psi_1 - \frac{\rho_1}{\rho_0} \nabla \cdot \mathbf{v}_0 \right). \quad (5.6)$$

The corresponding wave equation reads

$$\begin{aligned} & \partial_t \left\{ \partial_t \psi_1 + \mathbf{v}_0 \cdot \nabla \psi_1 - \frac{\alpha}{\rho_0} \left( \nabla^2 \psi_1 - \frac{\rho_1}{\rho_0} \nabla \cdot \mathbf{v}_0 \right) \right\} \\ & + \nabla \cdot \left\{ -\frac{\nabla \psi_1}{c^2} + \mathbf{v}_0 \left( \partial_t \psi_1 + \mathbf{v}_0 \cdot \nabla \psi_1 - \frac{\alpha}{\rho_0} \left( \nabla^2 \psi_1 - \frac{\rho_1}{\rho_0} \nabla \cdot \mathbf{v}_0 \right) \right) \right\} = 0. \end{aligned} \quad (5.7)$$

Taking into account that the background flow is incompressible,  $\nabla \cdot \mathbf{v}_0 = 0$ , the equation reduces to

$$\partial_t \left\{ \partial_t \psi_1 + \mathbf{v}_0 \cdot \nabla \psi_1 - \frac{\alpha}{\rho_0} \nabla^2 \psi_1 \right\} + \nabla \cdot \left\{ -c^2 \nabla \psi_1 + \mathbf{v}_0 \left( \partial_t \psi_1 + \mathbf{v}_0 \cdot \nabla \psi_1 - \frac{\alpha}{\rho_0} \nabla^2 \psi_1 \right) \right\} = 0. \quad (5.8)$$

Setting  $\alpha = 0$ , one recovers the non-viscous result of equation (2.18).

As a side note, observe equation (5.8) yields the d'Alembertian

$$\Delta \psi_1 = \frac{4}{3} \frac{\nu c}{\rho_0} (\partial_t + \mathbf{v}_0 \cdot \nabla) (c^{-2} \nabla^2 \psi_1), \quad (5.9)$$

which, under the definition of the four-velocity as  $V^\mu = \frac{(1; \mathbf{v})}{\sqrt{\rho_0 c}}$ , can be expressed as

$$\Delta \psi_1 = \frac{4}{3} \frac{\nu c^2}{\sqrt{\rho_0 c}} (V^\mu \nabla_\mu) (c^{-2} \nabla^2 \psi_1). \quad (5.10)$$

Thus, the wave equation results in a metric that is no longer Lorentz invariant:

$$g^{\mu\nu} = V^\mu V^\nu + \frac{c}{\rho} {}^{(3)}g^{\mu\nu}. \quad (5.11)$$

One should also inspect the effect of viscosity in the definition of specific enthalpy. Due to the irreversible modifications in the system viscosity induces, one can no longer claim entropy is conserved. Consequently, specific enthalpy assumes its most general form, as

$$dh = \frac{T}{\rho V} dS + \frac{dp}{\rho}. \quad (5.12)$$

When  $dS = 0$ , we obtain the formerly known definition of equation (2.8).

Working once more in a static fluid configuration, the wave equation (5.8) reads

$$\partial_t^2 \psi_1 - \left( \frac{\alpha}{\rho} \partial_t + c^2 \right) \nabla^2 \psi_1 = 0. \quad (5.13)$$

Again, the differentiating element is the viscous term in  $\alpha$ . Making use of the ansatz (4.2), one obtains the wave equation in terms of the radial field,

$$\partial_r^2 \varphi + \left( \frac{\omega^2}{c^2 - i\omega\alpha/\rho_0} - \frac{1}{r^2} \left( m^2 - \frac{1}{4} \right) \right) \varphi = 0, \quad (5.14)$$

from which we observe viscosity is only relevant when dealing with high frequencies  $\omega$ . The viscous term can be thought of as a correction to the local speed of sound. We define an effective local speed of sound,

$$c_{\text{eff}}^2 = c^2 - i \frac{\omega\alpha}{\rho_0}, \quad (5.15)$$

which can be cast to polar form,

$$c_{\text{eff}} = c\beta e^{i\theta}, \quad (5.16)$$

with

$$\beta = \left( 1 + \frac{\alpha^2 \omega^2}{\rho_0^2 c^4} \right)^{\frac{1}{4}}, \quad \sin \theta = \sqrt{\frac{\beta^2 - 1}{2\beta^2}}, \quad \cos \theta = \sqrt{\frac{\beta^2 + 1}{2\beta^2}}. \quad (5.17)$$

It is interesting to note that the wave equation obtained,

$$\partial_r^2 \varphi + \left( \frac{\omega^2}{c_{\text{eff}}^2} - \frac{1}{r^2} \left( m^2 - \frac{1}{4} \right) \right) \varphi = 0, \quad (5.18)$$

has a known analytical solution,

$$\varphi(r) = D_1 \sqrt{r} J_m(\omega r / c_{\text{eff}}) + D_2 \sqrt{r} Y_m(\omega r / c_{\text{eff}}), \quad (5.19)$$

in all identical to the solution for the non-viscous case, given by equation (4.4).

In view of analysing the role of viscosity in the analogue treatment, we first derive its units. Secondly, we define the range of realistic values in such units. Numerically, we work with  $c = \rho = 1$ . This choice is equivalent to rescaling the quantities

$$\hat{\omega} = \frac{\omega}{c}, \quad \hat{\alpha} = \frac{\alpha}{c\rho_0}, \quad (5.20)$$

resulting in the wave equation

$$\partial_r^2 \varphi(r) + \left( \frac{\hat{\omega}^2}{1 - i\hat{\alpha}\hat{\omega}} - \frac{1}{r^2} \left( m^2 - \frac{1}{4} \right) \right) \varphi(r) = 0. \quad (5.21)$$

In the following sections, we will be studying how superradiance and the instabilities are influenced by viscosity, and we want our simulations to reflect real viscous fluids. That can only be achieved by

matching  $\alpha$  with the viscosities of real fluids. Bearing that in mind, we proceed to dimensional analysis of  $\alpha$  in equation (5.18):

$$[\alpha] = \frac{M}{LT}, \quad (5.22)$$

where  $M$  is a mass unit,  $L$  stands for length and  $T$  for time. Equation (5.21) allows us to conclude on the units of the new viscosity parameter  $\hat{\alpha}$ ,

$$[\hat{\alpha}] = L. \quad (5.23)$$

A list of viscosities for some known fluids in these units can be found in Table 5.1. The choice of  $\text{cm}$  for length has to do with the experimental realisation of the setup; in particular with  $R_0 = 1 \text{ cm}$ . These orders

Material	$\alpha$ (Pa · s)	$\rho$ (kg/m <sup>3</sup> )	$c$ (m/s)	$\hat{\alpha}$ (cm)
Gasoline	$6.00 \times 10^{-6}$	700	1250	$6.86 \times 10^{-10}$
Mercury	$1.53 \times 10^{-3}$	13600	1420	$7.92 \times 10^{-9}$
Water	0.001	998	1480	$6.77 \times 10^{-8}$
Kerosene	$1.64 \times 10^{-3}$	810	1320	$1.53 \times 10^{-7}$
Linseed oil	0.033	820	1770	$2.28 \times 10^{-6}$
Glycerin	0.950	1260	1920	$3.93 \times 10^{-5}$
Castor Oil	0.650	961	1480	$4.57 \times 10^{-5}$

Table 5.1: Viscosity  $\hat{\alpha}$  of known materials at room temperature. We can observe that viscosities of typical fluids are, at most, of the order of  $\hat{\alpha} \sim 10^{-5} \text{ cm}$ .

of magnitude will serve as reference in the upcoming sections. All hats are dropped for the remainder of the chapter.

## 5.2 Wave dispersion relation

Following the prescription presented in Section 3.2, one obtains the equation:

$$c^2 \|\mathbf{k}\|^2 - \omega^2 + i\alpha \frac{\omega}{\rho} \|\mathbf{k}\|^2 = 0, \quad (5.24)$$

whose roots yield the dispersion relation

$$\omega = \frac{i\alpha \|\mathbf{k}\|^2 \pm \|\mathbf{k}\|^2 \sqrt{4c^2 \rho^2 - \|\mathbf{k}\|^2 \alpha^2}}{2\rho}. \quad (5.25)$$

Setting  $\alpha = 0$  produces the non-viscous result. Being the background fluid at rest, we do not obtain a Doppler correction as in the draining bathtub spacetime. Instead, some correction terms in the viscous parameter arise.

## 5.3 Scattering in the presence of viscosity

Working with the viscous wave equation (5.18), we start by deriving the condition for energy conservation. Following the demonstration in Reference [27], one can show the Wronskian associated with equation (5.18) is not constant. This result appears as a consequence of the effective potential in the

wave equation being complex. Consider a Schrodinger-like wave equation, of the form

$$\frac{d^2 y}{dx^2} + [V(x) + i\Gamma(x)] y = 0, \quad (5.26)$$

where  $y(x)$  is a scalar field and the effective potential is given by  $V(x) + i\Gamma(x)$ .  $V(x)$  and  $\Gamma(x)$  are real. The spatial derivative of the Wronskian reads

$$\frac{d}{dx}[W(y, y^*)] = \frac{d}{dx}(y\partial_x y^* - y^*\partial_x y) = y\partial_x^2 y^* - y^*\partial_x^2 y = 2i\Gamma|y|^2, \quad (5.27)$$

where we used equation (5.26) to substitute the second order derivatives. This result depends only on the imaginary part of the potential. Given a real effective potential,  $\Gamma(x) = 0$ , the Wronskian is constant in  $x$ , justifying the previous analysis. The effective potential of equation (5.18) is given by

$$\frac{\omega^2}{c^2 - i\omega\alpha/\rho_0} - \frac{1}{r^2} \left( m^2 - \frac{1}{4} \right), \quad (5.28)$$

which, in terms of  $V(r)$  and  $\Gamma(r)$ , can be expressed as

$$V = \frac{\omega^2 c^2}{c^4 + \left(\frac{\omega\alpha}{\rho}\right)^2} - \frac{1}{r^2} \left( m^2 - \frac{1}{4} \right) \quad (5.29)$$

$$\Gamma = \frac{\alpha\omega^3}{\rho c^4 + \frac{\omega^2 \alpha^2}{\rho}}. \quad (5.30)$$

Thus, one obtains the radial derivative of the Wronskian,

$$\frac{dW}{dr} = 2i \frac{\alpha\omega^3}{\rho c^4 + \frac{\omega^2 \alpha^2}{\rho}} |\varphi(r)|^2. \quad (5.31)$$

Integration in the radial coordinate yields

$$W(r') - W(R_0) = 2i \frac{\alpha\omega^3}{\rho_0 c^4 \beta^4} \int_{R_0}^{r'} dr |\varphi(r)|^2, \quad (5.32)$$

with  $\beta$  defined in equation (5.17). We considered the upper limit of integration to be a generic radius  $r'$ . In a scattering experiment, we study the unbounded system, where  $r' \rightarrow \infty$ . Later in the confined setup the integration limit is adjusted accordingly ( $r' = R_1$ ).

The Wronskian at  $R_0$  is still given by equation (4.9). The Wronskian at infinity is slightly modified. Actually, the behaviour of the viscous wave equation (5.18) is similar to the previous case, provided we substitute  $c \rightarrow c_{\text{eff}}$ . Hence, we write

$$W_\infty(\varphi, \varphi^\dagger) = \frac{2i\omega}{c_{\text{eff}}} (1 - |R_{\omega m}|^2). \quad (5.33)$$

The energy conservation condition reads

$$\frac{\omega}{c_{\text{eff}}} (1 - |R_{\omega m}|^2) - \rho_0 (\omega - m\Omega) \frac{\text{Re}(Z_{\bar{\omega}})}{|Z_{\bar{\omega}}|^2} |\varphi(R_0)|^2 = \frac{\alpha\omega^3}{\rho_0 c^4 \beta^4} \int_{R_0}^{\infty} dr |\varphi(r)|^2. \quad (5.34)$$

Due to the fact that the RHS of the equation is not zero, we obtain a modified condition for  $|R_{\omega m}|^2$  for a viscous superradiant system,

$$\omega < m\Omega \implies |R_{\omega m}|^2 > 1 - \alpha\omega^2. \quad (5.35)$$

When  $\alpha = 0$ , one recovers the non-viscous result. We have now returned to our units of  $\rho_0 = c = 1$ . In fact, we chose working with these variables explicitly in the above demonstration to avoid misplacing  $c_{\text{eff}}$ . Thus, one should look at the equations above with a critical eye, bearing in mind that whenever  $\rho_0$  or  $c$  are present we refer to  $\alpha$  in the standard units of  $\frac{\text{M}}{\text{LT}}$  and not to  $\hat{\alpha}$ . Note the corrections due the  $\alpha\omega^2$  term are not noticeable in this work, given the ranges of  $\alpha$  and  $\omega$  considered.

Identically to the previous chapters, we plot the reflection coefficient  $|R_{\omega m}|^2$  as a function of the frequency  $\omega$  – Figure 5.1. We work with  $\Omega = 0.9$  and  $\Omega = 3$  for both  $m = 1$  and  $m = 2$ , while varying the values of  $\alpha$  in accordance with the ranges presented in Table 5.1. One observes greater viscosity

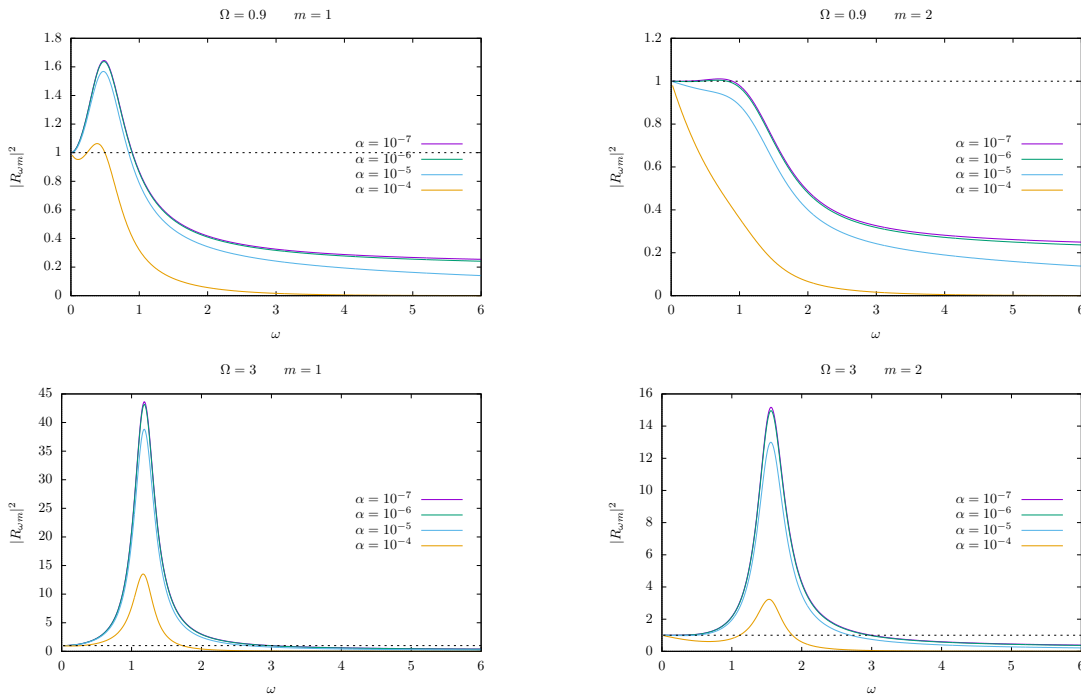


Figure 5.1: Reflection coefficient  $|R_{\omega m}|^2$  as a function of  $\omega$ . The plots presented here provide the modified solutions to Figure 4.1. For each pair of parameters  $(\Omega, m)$ , several orders of magnitude of  $\hat{\alpha}$  are studied. We observe increasing viscosity yields less amplification. In the range of viscosities of real fluids and the frequencies  $\omega$  considered, the superradiant limit is, in good approximation,  $|R_{\omega m}| = 1$ . As usual, we plot the limit above which superradiance occurs as a dashed line.

returns less amplification. This was to be expected, as a viscous fluid behaves as a dissipative means for energy. In order to quantitatively assess how viscosity impacts the reflection coefficient, we computed the areas associated with the various curves of Figure 5.1. This was done via an interpolating function that was then integrated. Afterwards, the areas were normalised to its respective no viscosity curve,

$$\text{Area normalisation} = \frac{\text{Area}(\alpha \neq 0)}{\text{Area}(\alpha = 0)}. \quad (5.36)$$

We obtained the results displayed in Figure 5.2.

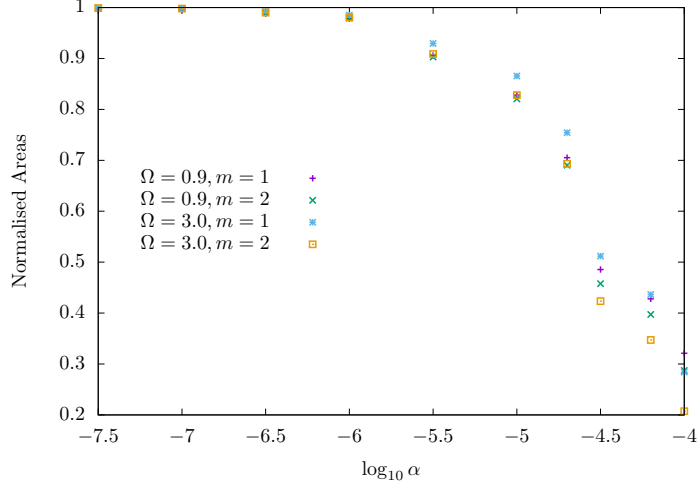


Figure 5.2: Area normalisation. For the same  $\Omega$ , viscosity's impact is higher for  $m = 2$ . One should pay special attention to the case where  $\alpha = 10^{-7}$ , as the ratio area with viscosity to area with no viscosity is virtually 1. This validates our previous approach of assuming water to have null viscosity. Recall that water has a viscosity of order of magnitude  $10^{-8}$ .

## 5.4 Quasinormal modes. Superradiant instabilities in the presence of viscosity

In the present section, we examine how viscosity affects the QNMs of the system. We start with the already known results for the non-viscous case, displayed in Table 4.2, and increase  $\alpha$  up to several orders of magnitude. An illustrative example of the QNMs for increasing viscosity at  $\Omega = 5$  and  $m = 1$  is displayed in Figure 5.3. Let us focus our attention in the behaviour of  $\omega_I$ . Being a positive number, it is

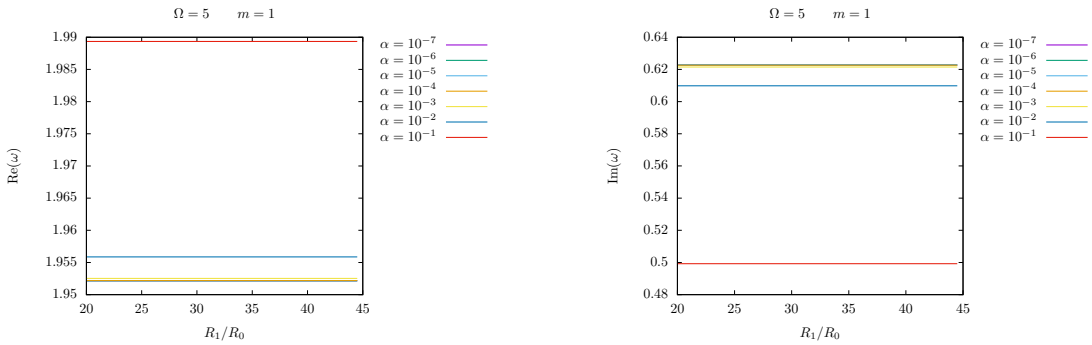


Figure 5.3: Real and imaginary parts of the frequency for the QNMs. We increase the viscosity parameter having as a starting point the previously detected  $\omega_{\text{QNM}}$  for  $\alpha = 0$ . Observe the colour code is kept in both plots. As viscosity increases,  $\omega_R$  increases and  $\omega_I$  decreases. This plot corresponds to  $\Omega = 5$ ,  $m = 1$ .

unstable. The fact that it decreases as viscosity increases means the amplification due to the instability is progressively less and less. Such is in agreement with the results of Figure 5.1. Notice, however, that modifications to the QNMs frequencies due to viscosity occur only for orders of magnitude greater than  $\alpha \sim 10^{-3}$ . As it happens, the QNMs frequencies of real fluids suffer no relevant changes due to viscosity. In Figure 5.4, we plot the QNMs frequency offset over different rotational speeds  $\Omega$ . The offset

is computed with respect to the frequencies of the corresponding QNMs in the absence of viscosity:

$$\omega_{\text{QNM}} \text{ offset} = \omega_{\text{QNM}}(\alpha = 0) - \omega_{\text{QNM}}(\alpha \neq 0). \quad (5.37)$$

Thus, the regressions found for Figure 4.9 are also applicable to realistic viscous fluids.

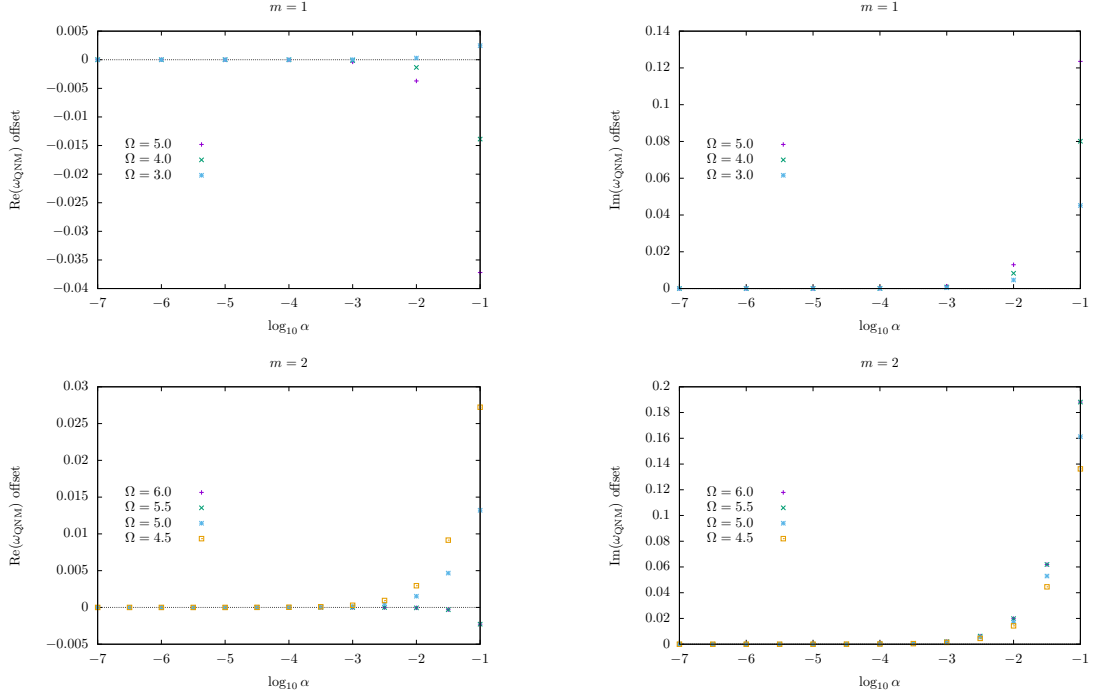


Figure 5.4: Offset of the real and imaginary parts of the frequency for the QNMs with respect to the non-viscous case. In the right panel we display the offset of real part of the frequency and on the left the imaginary. One can observe that the values for  $\omega_{\text{QNM}}$  only start to diverge from the non-viscous result for viscosities higher than  $\alpha \sim 10^{-3}$ .

## 5.5 Confined geometry in the presence of viscosity

At last, we examine whether viscosity plays a significant role in the subcritical flow velocities regime. In the previous chapter, we had seen that for small enough rotational speeds  $\Omega$ ,  $\omega_I$  was negative, changing signs afterwards. Running the same parameters as before, with  $\alpha \neq 0$ , one observes that, in the range of realistic viscosities, no modifications arise. In fact, not even higher viscosities of the order of  $\alpha \sim 10^{-2}$  result in any changes to the behaviour of the frequencies at subcritical speeds. For  $m = 2$ , however, one detects some effects at  $\alpha \sim 10^{-1}$ . Note that there are no changes for  $\omega_R$  for either  $m = 1$  or  $m = 2$ . In Figure 5.5, we have plotted the case of  $\Omega = 0.4$  as an example. Due to the constancy of the plots, we assume the fit of Figure 4.11 for the case of no viscosity to hold here as well. One thus concludes the behaviour of the frequencies for subcritical speeds is independent of viscosity, in the domain of real fluids.

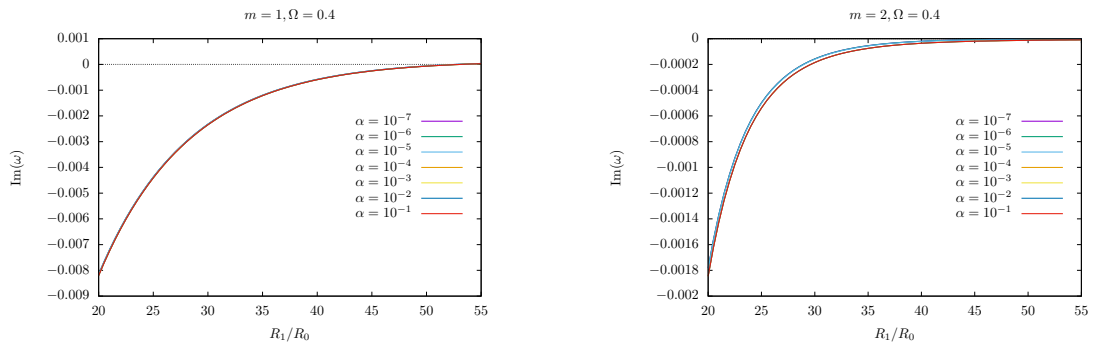


Figure 5.5: Imaginary part of the frequency as a function of the ratio  $R_1/R_0$ , for several values of viscosity. The rotational speed is kept constant at  $\Omega = 0.4$  while we evaluate the cases of  $m = 1$  and  $m = 2$ . The only noticeable change happens for  $m = 2$  at  $\alpha = 10^{-1}$ . No other changes are induced as all plots overlap.



# Chapter 6

## Conclusions

### 6.1 Achievements

Albert Einstein's GR is a colossal achievement of 20th-century physics. The claim that what we perceive as the force of gravity actually arises from the curvature of spacetime is not a straightforward one. The scientific paradigm Einstein introduced is still present nowadays, with GR being our best candidate for a theory of gravity. Since its initial publishing, GR has been subjected to many experimental tests. The most recent triumph was in 2015 with the detection of gravitational waves, a century after their initial prediction. GR is a very hard theory to test at will. Besides its mathematically challenging predictions, the experimental tests must be done under very specific conditions. Tests of strong-field gravity, for instance, can only be performed near astrophysical bodies such as BHs and neutron stars. Probing this type of results is not an easy task and it often deems itself impossible due to technological lags. Acoustic analogues bridge the gap between theory and experiment. Research on the area sheds new light on BH physics. It allows for the testing of phenomena like Hawking radiation and superradiance, to name but a few. Such effects are virtually impossible to study in astrophysical BHs with the existing technology.

Throughout this work we studied the analogue gravity description of rotating BHs, with a focus on superradiance. We analysed two distinct spacetimes: the draining bathtub and the rotating cylinder setups. Following the description in Reference [19], we showed the mathematical correspondence between fluid mechanics and GR. By working with the continuity and the Euler equations, one is able to derive a wave equation which completely determines the propagation of acoustic disturbances, characterised by  $(p_1, \rho_1, \psi_1)$ . The background fields  $(p_0, \rho_0, \psi_0)$ , which appear as time-dependent and position-dependent coefficients in the equation, are constrained to solve the equations of fluid motion for an externally-driven, barotropic, inviscid and irrotational flow. Observe  $p$ ,  $\rho$  and  $\psi$  are respectively the pressure, the density and the velocity potential fields of the fluid. These physical quantities are our bread and butter in studying wave propagation.

As a first approach, we work with a  $(1+2)$ -dimensional draining bathtub potential. One solves the differential wave equation numerically, by iteratively integrating the wave equation for different frequencies  $\omega$ . The boundary conditions imposed are the analytical solutions of the wave equation at the horizon

and at infinity. The output of each cycle consists of a pair of points  $(\omega, |R_{\omega m}|^2)$ , which is later plotted. The reflection coefficient  $|R_{\omega m}|^2$  – defined as the ratio in energies between reflected and incident waves – allows one to conclude about the occurrence of superradiant scattering. In fact, the superradiance condition  $\omega < m\Omega$  yields  $|R_{\omega m}|^2 > 1$ . Observe this arises from the fact that the Wronskian associated to the wave equation is constant in the radial coordinate. Lastly, one computes the QNMs of the system. The results obtained are consistent with existing literature – cf. References [21] and [23]. One of the big issues with this proposal is at the experimental level. Non-linear effects such as turbulence may arise at supersonic rotational speeds, invalidating the theoretical description. Alternatively, we explore a different setup where this problem does not occur.

The new setup consists of a rotating cylinder as possible source of amplification. A static fluid configuration is assumed. We make use of a quantity called acoustic impedance to describe the interaction between the wave and the wall of the cylinder. The acoustic impedance is set to  $Z = 1 - i$ , a standard value for known materials. Similarly to the vortex spacetime, we derive a wave equation which is solved numerically. We plot the reflection coefficient against the wave frequency and observe superradiant scattering in certain domains of  $\omega$ . This result shows that superradiance may arise in spacetimes with no horizons. Another interesting conclusion worth mentioning is that the amplification is bounded from above: at subsonic rotational speeds,  $|R_{\omega m}|^2$  is never larger than 2. This restriction is present in a wide class of theories and geometries, from which the scattering of charged scalar off Kerr BHs is an example. Analysis of the QNMs of the system shows that the solutions are unstable. We argue for a correlation between the QNMs and the location of the maximum amplification. A linear regression set to determine the QNM frequencies given the cylinder rotational speed is also provided. At last, one observes stable solutions exist in confined geometries. The critical point of vanishing  $\omega_I$  depends on both the confinement radius and the cylinder velocity.

With the goal of expanding the treatment onto more realistic fluids, one introduces viscosity. At the level of the governing equations, that means we work with the Navier-Stokes equation rather than with the Euler equation. A new wave equation is derived. Using dimensional analysis, we evaluate the range of realistic viscosity values. A core feature of the viscous wave equation is its complex effective potential. One shows this produces a Wronskian that is no longer conserved. We determine the value of  $\frac{dW}{dr}$  and use it to write a new energy conservation equation. Applying the superradiance condition to the aforementioned equation yields  $|R_{\omega m}|^2 > 1 - \alpha\omega^2$ . Note the correction term  $\alpha\omega^2$  is negligible given the domains of  $\alpha$  and  $\omega$  considered in this thesis. The only relevant modification to the results due to viscosity happens in the superradiant scattering. We see that larger values of viscosity yield smaller and smaller amplifications. This is accordance with the idea that viscosity goes hand-in-hand with energy dissipation. On a final note, the impact of viscosity is quantitatively evaluated when we normalise the areas below the reflection curves.

## 6.2 Future work

Many possible extensions to this work are possible. We list some of them here. First of all, we rely on linear perturbation theory. When the perturbations to the variables  $(p, \rho, \psi)$  are introduced, in equation (2.10), one only works up to first order terms in  $\varepsilon$ . At high rotational speeds – namely at supersonic rotational speeds –, this description does not suffice and higher order terms are required. Non-linear effects are very difficult, if not impossible, to analyse from a purely analytical point of view. That is why one resorts to numerical simulations with higher order terms. Furthermore, one should look at the modifications induced in the vortex wave equation due to viscosity. We expect viscosity to play an important role near the centre of the drain, where the fluid velocity is higher. This makes the task of defining the event horizon of the experimental setup harder. Experimentally, we observe atypical behaviours of  $v_\theta(r)$ , where the velocity profile deviates from the usual  $1/r$  profile at small radial coordinates – cf. Reference [12]. A more complete description of the spacetime, with viscosity, could perhaps explain this result.

Regarding the cylinder setup, no experimental results have been produced yet. The first comparisons between theory and experiment should appear within the next couple of years. Only then can one look at the predictions produced in this work critically. For now, we call the reader's attention to some approximations and considerations assumed in this thesis that can be refined. In the viscous flow regime, rather than just assuming a static fluid configuration, one can produce a more accurate velocity profile. In fact, the background fluid is not at rest near the cylinder wall. In the confined setup, for instance, one can define the boundary conditions  $v(t, R_0) = \Omega R_0$  and  $v(t, R_1) = 0$ . This is due to the no-slip condition, which dictates the fluid has zero velocity relative to the solid boundaries. One possible description is provided by Ekman theory. Observe one needs not to consider the no-slip condition in cases where viscosity is not present. The approach in Chapter 5 works provided the measurements are made far enough from the radius of rotation  $R_0$ . However, "far enough" is ill-defined here. Only by refining the velocity profile can we validate the results obtained. Yet another interesting extension of the work would be modifying the values of acoustic impedance. We explored the results for the standard  $Z = 1 - i$  value, but did not see how sensitive the results were to slight modifications (within the same order of magnitude). Take, for example, the upper bound of  $|R_{\omega m}|^2 = 2$  for subcritical rotational speeds. Is it modified? Another challenging task would be extending the analytical treatment further. In particular, one could solve the cylinder – with and without viscosity – wave equations to arrive at an analytical expression for the reflection coefficient.



# Bibliography

- [1] R. Ruffini and J. A. Wheeler. Introducing the black hole. *Phys. Today*, 24(1):30, 1971. doi: 10.1063/1.3022513.
- [2] F. W. Dyson, A. S. Eddington, and C. Davidson. A determination of the deflection of light by the sun's gravitational field, from observations made at the total eclipse of may 29, 1919. *Philosophical Transactions of the Royal Society of London A: Mathematical, Physical and Engineering Sciences*, 220(571-581):291–333, 1920. ISSN 0264-3952. doi: 10.1098/rsta.1920.0009.
- [3] B. P. Abbott et al. Observation of Gravitational Waves from a Binary Black Hole Merger. *Phys. Rev. Lett.*, 116(6):061102, 2016. doi: 10.1103/PhysRevLett.116.061102.
- [4] K. Schwarzschild. On the gravitational field of a mass point according to Einstein's theory. *Sitzungsber. Preuss. Akad. Wiss. Berlin (Math. Phys.)*, 1916:189–196, 1916.
- [5] P. O. Mazur. Black hole uniqueness theorems. 2000.
- [6] W. Israel. Event horizons in static vacuum space-times. *Phys. Rev.*, 164:1776–1779, 1967. doi: 10.1103/PhysRev.164.1776.
- [7] W. Israel. Event horizons in static electrovac space-times. *Commun. Math. Phys.*, 8:245–260, 1968. doi: 10.1007/BF01645859.
- [8] C. A. Manogue. The klein paradox and superradiance. *Annals of Physics*, 181(2):261 – 283, 1988. ISSN 0003-4916. doi: [http://dx.doi.org/10.1016/0003-4916\(88\)90167-4](http://dx.doi.org/10.1016/0003-4916(88)90167-4).
- [9] J. D. Bekenstein. Black holes and entropy. *Phys. Rev.*, D7:2333–2346, 1973. doi: 10.1103/PhysRevD.7.2333.
- [10] R. Brito, V. Cardoso, and P. Pani. Superradiance. *Lect. Notes Phys.*, 906:pp.1–237, 2015. doi: 10.1007/978-3-319-19000-6.
- [11] W. G. Unruh. Experimental black hole evaporation. *Phys. Rev. Lett.*, 46:1351–1353, 1981. doi: 10.1103/PhysRevLett.46.1351.
- [12] T. Torres, S. Patrick, A. Coutant, M. Richartz, E. W. Tedford, and S. Weinfurter. Observation of superradiance in a vortex flow. 2016.

- [13] R. Schutzhold and W. G. Unruh. Gravity wave analogs of black holes. *Phys. Rev.*, D66:044019, 2002. doi: 10.1103/PhysRevD.66.044019.
- [14] V. Cardoso, A. Coutant, M. Richartz, and S. Weinfurter. Detecting Rotational Superradiance in Fluid Laboratories. *Phys. Rev. Lett.*, 117(27):271101, 2016. doi: 10.1103/PhysRevLett.117.271101.
- [15] C. Pelloquin, L.-P. Euvé, T. Philbin, and G. Rousseaux. Analog wormholes and black hole laser effects in hydrodynamics. *Phys. Rev.*, D93(8):084032, 2016. doi: 10.1103/PhysRevD.93.084032.
- [16] J. Steinhauer. Observation of self-amplifying Hawking radiation in an analog black hole laser. *Nature Phys.*, 10:864, 2014. doi: 10.1038/NPHYS3104.
- [17] J. L. Gaona-Reyes and D. Bermudez. The theory of optical black hole lasers. *Annals Phys.*, 380: 41–58, 2017. doi: 10.1016/j.aop.2017.03.005.
- [18] A. Roldán-Molina, A. S. Nunez, and R. Duine. Magnonic Black Holes. *Phys. Rev. Lett.*, 118(6): 061301, 2017. doi: 10.1103/PhysRevLett.118.061301.
- [19] M. Visser. Acoustic black holes: Horizons, ergospheres, and Hawking radiation. *Class. Quant. Grav.*, 15:1767–1791, 1998. doi: 10.1088/0264-9381/15/6/024.
- [20] O. Ganguly. Acoustic superradiance in a slightly viscous fluid. 2017.
- [21] E. Berti, V. Cardoso, and J. P. S. Lemos. Quasinormal modes and classical wave propagation in analogue black holes. *Phys. Rev.*, D70:124006, 2004. doi: 10.1103/PhysRevD.70.124006.
- [22] S. Chandrasekhar and S. Detweiler. The quasi-normal modes of the Schwarzschild black hole. *Proc. Roy. Soc. Lond. A344*, pages 441–452, 1975.
- [23] V. Cardoso, J. P. S. Lemos, and S. Yoshida. Quasinormal modes and stability of the rotating acoustic black hole: Numerical analysis. *Phys. Rev.*, D70:124032, 2004. doi: 10.1103/PhysRevD.70.124032.
- [24] S. Rienstra and A. Hirschberg. An introduction to acoustics.
- [25] M. Delany and E. Bazley. Acoustical properties of fibrous absorbent materials. *Applied Acoustics*, 3(2):105 – 116, 1970. ISSN 0003-682X. doi: [http://dx.doi.org/10.1016/0003-682X\(70\)90031-9](http://dx.doi.org/10.1016/0003-682X(70)90031-9).
- [26] V. Baibhav, V. Cardoso, and R. Emparan. Universal bounds on superradiance (unpublished).
- [27] M. Richartz, S. Weinfurter, A. J. Penner, and W. G. Unruh. General universal superradiant scattering. *Phys. Rev.*, D80:124016, 2009. doi: 10.1103/PhysRevD.80.124016.
- [28] S. M. Carroll. *Spacetime and geometry: An introduction to general relativity*. 2004. ISBN 0805387323, 9780805387322.
- [29] C. W. Misner, K. S. Thorne, and J. A. Wheeler. *Gravitation*. W. H. Freeman, San Francisco, 1973. ISBN 9780716703440.

- [30] D. Griffiths. *Introduction to Quantum Mechanics*. Pearson international edition. Pearson Prentice Hall, 2005. ISBN 9780131118928.
- [31] G. Arfken and H. Weber. *Mathematical methods for physicists*. Elsevier Acad. Press, 2008. ISBN 9780120598762.
- [32] L. D. Landau and E. M. Lifshitz. *Fluid Mechanics, Second Edition: Volume 6 (Course of Theoretical Physics)*. Course of theoretical physics / by L. D. Landau and E. M. Lifshitz, Vol. 6. Butterworth-Heinemann, 2 edition, Jan. 1987. ISBN 0750627670.
- [33] F. Belgiorno and S. L. Cacciatori. Stimulated emission in black holes and in analogue gravity. *Gen. Rel. Grav.*, 48(11):145, 2016. doi: 10.1007/s10714-016-2140-4.
- [34] B. Cropp, S. Bhattacharya, and S. Shankaranarayanan. Hints of quantum gravity from the horizon fluid. *Phys. Rev.*, D95(2):024006, 2017. doi: 10.1103/PhysRevD.95.024006.
- [35] M. Krumm, H. Barnum, J. Barrett, and M. P. Mueller. Thermodynamics and the structure of quantum theory. *New J. Phys.*, 19(4):043025, 2017. doi: 10.1088/1367-2630/aa68ef.
- [36] R. Dey, S. Liberati, and R. Turcati. AdS and dS black hole solutions in analogue gravity: The relativistic and non-relativistic cases. *Phys. Rev.*, D94(10):104068, 2016. doi: 10.1103/PhysRevD.94.104068.
- [37] A. E. Gumrukcuoglu, K. Koyama, and S. Mukohyama. Role of matter in extended quasidilaton massive gravity. *Phys. Rev.*, D94(12):123510, 2016. doi: 10.1103/PhysRevD.94.123510.
- [38] L. Motl and A. Neitzke. Asymptotic black hole quasinormal frequencies. *Adv. Theor. Math. Phys.*, 7(2):307–330, 2003. doi: 10.4310/ATMP.2003.v7.n2.a4.
- [39] L. Motl. An Analytical computation of asymptotic Schwarzschild quasinormal frequencies. *Adv. Theor. Math. Phys.*, 6:1135–1162, 2003.
- [40] R. M. Wald. The thermodynamics of black holes. In *Lectures on quantum gravity. Proceedings, School of Quantum Gravity, Valdivia, Chile, January 4-14, 2002*, pages 1–37, 2002.
- [41] M. Orignotti, S. Bar-Ad, A. Szameit, and V. Fleurov. Analogue gravity by an optical vortex. Resonance enhancement of Hawking radiation. 2017.
- [42] D. N. Page. Hawking emission and black hole thermodynamics. In *Recent developments in theoretical and experimental general relativity, gravitation and relativistic field theories. Proceedings, 11th Marcel Grossmann Meeting, MG11, Berlin, Germany, July 23-29, 2006. Pt. A-C*, pages 1503–1507, 2006. doi: 10.1142/9789812834300\_0180.
- [43] J. M. Bardeen, B. Carter, and S. W. Hawking. The Four laws of black hole mechanics. *Commun. Math. Phys.*, 31:161–170, 1973. doi: 10.1007/BF01645742.
- [44] E. Mc Caughey. Hawking radiation screening and Penrose process shielding in the Kerr black hole. *Eur. Phys. J.*, C76(4):179, 2016. doi: 10.1140/epjc/s10052-016-4028-6.

- [45] G. 't Hooft. On the Quantum Structure of a Black Hole. *Nucl. Phys.*, B256:727–745, 1985. doi: 10.1016/0550-3213(85)90418-3.
- [46] R. P. Kerr. Gravitational field of a spinning mass as an example of algebraically special metrics. *Phys. Rev. Lett.*, 11:237–238, 1963. doi: 10.1103/PhysRevLett.11.237.
- [47] R. Penrose and R. M. Floyd. Extraction of rotational energy from a black hole. *Nature*, 229:177–179, 1971.
- [48] W. G. Unruh. Sonic analog of black holes and the effects of high frequencies on black hole evaporation. *Phys. Rev.*, D51:2827–2838, 1995. doi: 10.1103/PhysRevD.51.2827.
- [49] W. G. Unruh. Notes on black hole evaporation. *Phys. Rev.*, D14:870, 1976. doi: 10.1103/PhysRevD.14.870.
- [50] M. Visser. Dirty black holes: Thermodynamics and horizon structure. *Phys. Rev.*, D46:2445–2451, 1992. doi: 10.1103/PhysRevD.46.2445.
- [51] M. Visser. Dirty black holes: Entropy as a surface term. *Phys. Rev.*, D48:5697–5705, 1993. doi: 10.1103/PhysRevD.48.5697.
- [52] N. Andersson, P. Laguna, and P. Papadopoulos. Dynamics of scalar fields in the background of rotating black holes. 2. A Note on superradiance. *Phys. Rev.*, D58:087503, 1998. doi: 10.1103/PhysRevD.58.087503.
- [53] C. Barcelo, S. Liberati, and M. Visser. Analogue gravity. *Living Rev. Rel.*, 8:12, 2005. doi: 10.12942/lrr-2005-12. [Living Rev. Rel.14,3(2011)].
- [54] B. Gonzalez-Fernandez and A. Camacho. Fluid–Gravity Correspondence under the presence of viscosity. *Mod. Phys. Lett.*, A27:1250185, 2012. doi: 10.1142/S0217732312501854.
- [55] S. Weinfurtner, E. W. Tedford, M. C. J. Penrice, W. G. Unruh, and G. A. Lawrence. Classical aspects of Hawking radiation verified in analogue gravity experiment. *Lect. Notes Phys.*, 870:167–180, 2013. doi: 10.1007/978-3-319-00266-8.8.
- [56] K. P. Y. Thebault. *What Can We Learn From Analogue Experiments?* 2016.
- [57] M. Visser, C. Barcelo, and S. Liberati. Analog models of and for gravity. *Gen. Rel. Grav.*, 34: 1719–1734, 2002. doi: 10.1023/A:1020180409214.
- [58] V. Cardoso, S. Yoshida, O. J. C. Dias, and J. P. S. Lemos. Late time tails of wave propagation in higher dimensional space-times. *Phys. Rev.*, D68:061503, 2003. doi: 10.1103/PhysRevD.68.061503.
- [59] S. Robertson and G. Rousseaux. Viscous dissipation of surface waves and its relevance to analogue gravity experiments. 2017.

- [60] E. Berti, V. Cardoso, and A. O. Starinets. Quasinormal modes of black holes and black branes. *Class. Quant. Grav.*, 26:163001, 2009. doi: 10.1088/0264-9381/26/16/163001.
- [61] H. Kim. The Absence of fermionic superradiance (a simple demonstration). *JCAP*, 0811:007, 2008. doi: 10.1088/1475-7516/2008/11/007.



# Appendix A

## The potential barrier

In this section we discuss why larger values of the azimuthal number  $m$  yield smaller reflection coefficients in scattering experiments. We focus our analysis to two physical quantities encoded in the wave equation: the potential barrier and the energy.

The study is done using the draining bathtub spacetime. Recall the vortex wave equation, originally presented in equation (3.11), reads

$$H_{r_*, r_*} + Q(r)H = 0, \quad (\text{A.1})$$

where

$$Q = \left( \omega - \frac{Bm}{r^2} \right)^2 - V(r) \quad (\text{A.2})$$

$$V = \frac{r^2 - 1}{r^2} \left( \frac{1}{r^2} \left( m^2 - \frac{1}{4} \right) + \frac{5}{4r^4} \right). \quad (\text{A.3})$$

Note we are working with the rescaled quantities, with the hats dropped.

The one-dimensional time-independent Schroedinger equation reads

$$\partial_r^2 \Psi + (E - V)\Psi = 0, \quad (\text{A.4})$$

where  $E$  is the energy carried by the wave and  $V$  is the potential barrier. Depending on the behaviour of the energy with respect to the potential, the wave propagation falls under one out of two possible categories: scattering and bound states. First of all, one should mention the energy cannot be smaller than the potential in all domain; there is no possible solution for the wave equation. However, if the following situation occurs,

$$\begin{cases} E < V(+\infty) \\ E < V(-\infty), \end{cases} \quad (\text{A.5})$$

we are in the presence of bound states. Otherwise, a scattering experiment takes place. Such is the case in this thesis.

Establishing the connection between the standard Schrodinger equation and the draining bathtub wave equation, we arrive at:

$$\text{Energy: } \left( \omega - \frac{Bm}{r^2} \right)^2, \quad (\text{A.6})$$

$$\text{Potential barrier: } V(r) = \frac{(r^2 - 1)}{r^2} \left( \frac{1}{r^2} \left( m^2 - \frac{1}{4} \right) + \frac{5}{4r^4} \right). \quad (\text{A.7})$$

Below we plot the potential and test energies for the cases  $m = 1$  and  $m = 2$ .

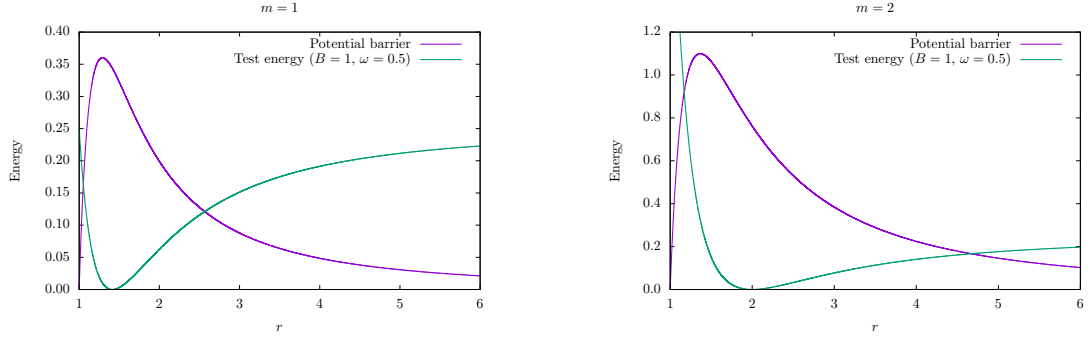


Figure A.1: Potential and test energies for the different values of  $m$ . We set  $B = 1$  and  $\omega = 0.5$  on both test energies.

One will show how these two plots can be analysed together. Allow us to take a step back, to a simpler scattering experiment. We make use of two test energies, both constant. See Figure A.2. The

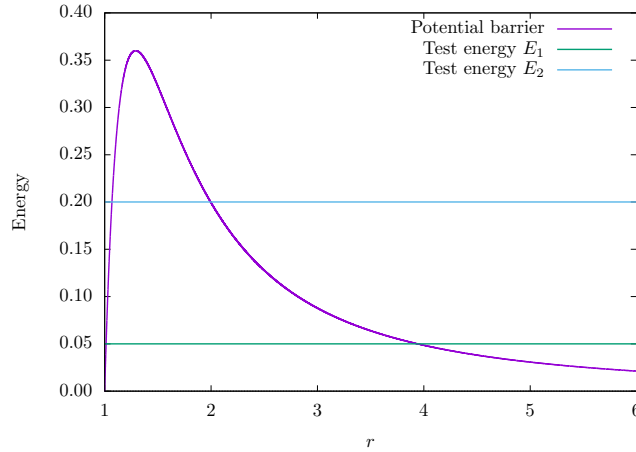


Figure A.2: Scattering experiment with two different incoming waves, carrying  $E_1$  and  $E_2$ . Observe  $E_2 > E_1$ .

potential has less influence on  $E_2$ , as  $E_2 > E_1$ . In fact, because the wave represented by the blue line carries more energy, it is subjected to less tunnelling. Consequently, the reflection coefficient is greater in  $E_2$ . For a more detailed explanation on quantum tunnelling, bound states and scattering, please refer to Reference [30].

The plots from Figure A.1 may be adapted so that we are able to use similar arguments. In particular, one can normalise the energy-potential intersection point to the maximum potential on both  $m = 1$  and

$m = 2$ . We organise the relevant coordinates in Table A.1.

Point	$m = 1$	$m = 2$
Intersection	(2.57, 0.12)	(4.67, 0.17)
Maximum	(1.29, 0.36)	(1.37, 1.10)

Table A.1: Points of interest from Figure A.1. The coordinates are displayed in the form of  $(r, V(r))$ . Note we are only interested on the intersection point on the right, as it accounts for the moment when the incoming wave first encounters the potential barrier.

The ratio intersection-maximum in  $V(r)$  is

$$m = 1 \quad \longrightarrow \quad 0.336475,$$

$$m = 2 \quad \longrightarrow \quad 0.151611.$$

We can think of this normalisation as the points where the energy curves intersect a potential barrier with maximum  $V(r) = 1$ . The  $m = 1$  curve intersects at a higher energy. In a simplified view, it corresponds to  $E_2$  in Figure A.2. As previously stated, this yields a greater reflection coefficient. Hence, larger amplification results from smaller  $m$ . This conclusion is in accordance with the numerical results.

Lastly, note this argument is extensible to the cylinder spacetime. Actually, that case is even simpler, as the energy depends only on  $\omega$  – see equation (4.3).